UNIVERSITY OF THESSALY

POLYTECHNIC SCHOOL

DEPARTMENT OF MECHANICAL ENGINEERING

LABORATORY OF MATERIALS

Diploma Thesis

Microstructural study of the HAZ and the effect of post weld

heat treatments on aluminum alloy 7005

By

Emmanouil G. Sariklakis

Supervisor:

Dr. Helen Kamoutsi

Submitted for the Partial Fulfillment of the requirements for

the degree of Diploma in Mechanical Engineering

Certified by the members of the Thesis Committee:

First Examiner   Dr. Helen Kamoutsi

(Supervisor)   Lab Teaching Staff

                        Department of Mechanical Engineering

                        University of Thessaly

Second Examiner   Dr. Nikolaos Aravas

                   Professor of Computational Mechanics of Structures

                   Department of Mechanical Engineering

                   University of Thessaly

Third Examiner   Dr. Alexis Kermanidis

                   Associate Professor of Mechanical Behaviour of Metallic Materials

                   Department of Mechanical Engineering

                   University of Thessaly

Contents

Table of tables

Table of Figures

8

Acknowledgements

The present project was performed in order to satisfy the requirements of the degree of Diploma in Mechanical Engineering at University of Thessaly.

Initially, I would like to express my gratefulness to my superior Dr. Helen Kamoutsi, whose scientific background and perception were determining factors of setting the methodology and the experiments of the research.

Furthermore, I would like to express my gratitude to Professor Nikolaos Aravas and Associate Professor Alexis Kermanidis for accepting to participate in the three-member evaluation committee of my Diploma Thesis.

Lastly, special thanks are extended to all the members of the Laboratory of Materials, both students and professors whose aid helped me adjust in the Laboratory.

Abstract

An experimental study of the effect of post weld heat treatment in 7005 aluminum alloys is presented in this Diploma Thesis. Also, a simulation of the heat affected zone of the 7005 alloy in order to examine its behavior at each peak temperature was performed. Furthermore, metallographic analysis of 7005 and 7020 alloys was conducted, as well as microhardness measurements (profiles) for welds of 7005 of T1 and T6 heat treatment and 7020-T6 aluminum alloys. The results of this experiment have shown that the microhardness of the welded alloys is affected by the initial microstructure. Moreover, the post weld heat treatment is an effective method of restoring the microhardness of the HAZ areas of the metal, softened by the heat. Finally, we can categorize the heat affected zone in two subdivisions depending the hardness mechanisms. The overageing zone and the dissolution zone. The overageing zone consists of precipitates that have grown in temperatures between 300°C and 400°C. The dissolution zone consists of dissolution precipitates that form for temperatures over 400°C.

1 Introduction

In the recent years, there has been great technological development in cycling because of the demand for maximum performance for every bicycle component from both professional and amateur cyclists. For this reason, manufacturing companies use more and more sophisticated materials to optimize the strength-weight ratio and satisfy those requirements. The most common of them is the aluminum and more specifically its alloys because it is a cheap and easy to machine material especially compared to titanium and carbon fiber. Also, aluminum's strength-weight ratio is better that the one of steel.

The Aluminum alloys are classified by the International Alloy Designation System as it is presented in Chapter 2. Specifically, the alloys of 7000 series are widely used for bicycle frames because of their high fatigue resistance which is achieved by the appropriate heat treatment. This heat treatment develops thin reinforcement precipitates for this purpose [1].

In bicycle frame applications, it is necessary to join of the alloys, using an appropriate welding process. Changes in the microstructure of the alloy can occur inside the weld metal, heat-affected zones and even unaffected zones. Also, changes in mechanical properties are created by welding heat input. Therefore, the effect of welding on the material properties is an important consideration. Furthermore, the heat treatment of the aluminum alloy, that is used as frame, before the welding is also important as it causes solid solution and precipitation that affects the weldability of the alloy.

1.1 Description of the problem.

In the present work alloys 7005 and 7020 were obtained in order to be considered for the use of a bicycle frame. The 7005-alloy material was obtained in 2 cylindrical pipes in order to to be welded with thickness 3.2mm. Each of the pipes was obtained from a different supplier and with different thermal process. The first one has been processed through T6 heat treatment and the second one through T1 heat treatment. The 7020 alloy was obtained in a welded plate form. The different heat treatments that the two 7005-alloy materials have received affect differently their microstructures raising the question of whether those two be welded even if they are from the same alloy. Also, the welding of a 7020 alloy is examined. The heat affected zone of the weldings was also studied thoroughly.

1.2 Thesis objective

Considering those data, the present thesis studies the heat treatment and the welding areas of these two alloys as well as post heat treatment methods. More specific the thesis objectives are the following.

1. To study the effects of the different heat treatments in the microstructure of the alloys.

2. To study the effects of the welding zones in the microstructure and microhardness of the materials.
3. To simulate the heat affected zone of the metal with appropriate heat treatments.
4. To optimize the hardness of the heat affected zone
5. To present a link between thermodynamic calculations and phase equilibria of the two alloys.

1.3   Thesis methodology

The study is focused on 7005 aluminum alloy and 7020 aluminum alloy of the 7xxx series, the T1 and T6 heat treatment methods and the welding zones. The experimental procedure includes the following actions.

1. Heat treatments
2. Metallography
3. Image analysis
4. Microhardness tests
5. Thermodynamics calculations (Thermocalc TCAL5)

1.4   Thesis outline

The thesis outline is the following

Chapter 1. Introduction

Chapter 2. Literature review

Chapter 3. Experimental procedure

Chapter 4. Results and Discussion

Chapter 5. Conclusions

2 Literature review

The literature review starts with a brief introduction on aluminum alloys (classification and designation) and the heat treatments that are suggested for improving their mechanical properties. It continues with a discussion of strengthening mechanisms of the aluminum alloys and there is a discussion of the ageing process and the effects it causes in the microstructure of the alloys. One more subject that is also presented is the welding of aluminum alloys. Finally, there is a thermodynamic description of the Al-Mg-Zn system.

2.1 Aluminum Alloys

"Light Metals" is a group of metals that has been named after their ability to reduce the weight of the structures that they are used for constructing. Aluminum alloys belong to this metal group and therefore are appropriate for "light" weight structures [2].
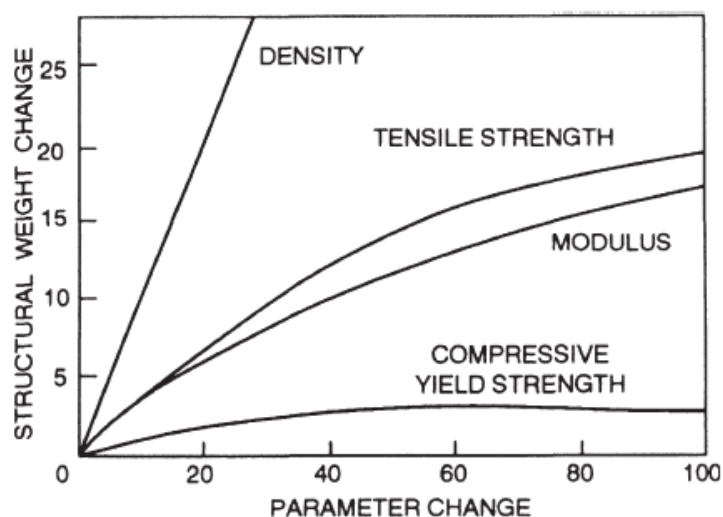
Figure 1: Property improvement effect on the structural weight [2].

There are two main classifications of aluminum alloys: wrought alloys and casting alloys. There is also a further subsection into heat-treatable and non-heat-treatable alloys [3].

2.2 Designation of wrought aluminum alloys

Alloys 7005 and 7020 belong to the 7xxx series of Al-Mg-Zn heat treatable wrought alloys and are commonly used for bicycle frames and other transportation applications.

The naming of the wrought alloys is given by the International Alloy Designation System. There is a four-digit number for each alloy; The first digit indicates the major alloying elements, the second one the variation of the alloy, and the third and fourth digits specifies the alloy in the series [3, 4].

Table 1: Designation System of Wrought Aluminum alloys based in the main alloying element.

- The 2xxx series are basically alloyed with cooper and are categorized as heat treatable.

- The 3xxx series has as main alloying element the manganese and are strain hardenable.
- The 4xxx series alloys are based on silicon and can be heat treatable or not, depending on the amount of silicon and the other alloying elements
- The 5xxx series have as main alloying element the magnesium and are strain hardenable.
- The 6xxx series alloys have both magnesium and silicon as base alloying elements and are heat treatable.
- The 7xxx series alloys are based on zinc, often with significant amounts of copper and magnesium, and they are heat treatable.
- The 8xxx series contain several less frequently used major alloying elements like iron. Their characteristics depend on the major alloying element [5].

2.3 Temper designation system for wrought alloys

For the heat treatment of all forms of wrought aluminum alloys there is a naming system of EN 515. According to this system;

- The main letters that designate the treatment are F, O, H, W, T.
- Following the main letter extra digits are used to define other sub-sections of the main tempers, indicating the sequence that the treatment follows.
- If there is a need for further thermo-mechanical procedures, extra digits can be added with the result of different characteristics [3].

Standard tempers can be defined by the next terms.

- Cold working: The plastic deformation of the metal occurs at this temperature and the rate at which the strain hardening takes place.
- Strain-hardening: Formation of a metal structure by cold working treatment that results in increased strength and hardness with loss of plasticity.
- Solution heat-treatment: Heat treatment during which the specimens are heated to a suitable temperature, maintaining this temperature high enough to allow the ingredients to enter the solid solution and cooling fast enough to keep them in solution.
- Ageing: Precipitation from supersaturated solid solution that changes the properties of the alloy. This can take part in two ways depending from the temperature (natural ageing for slow-room temperatures or artificial ageing for fast-high temperatures).
- Annealing: The heat treatment that softens the metal by removing the strain-hardens or by depositing precipitates from the solid solution.

The use of the letters that were mentioned above are presented in the following paragraph.

- <u>F Temper</u> (Material As fabricated): There aren't specified any mechanical property boundaries.
- <u>0 Temper</u> (Material Annealed)**:** In order to get the minimum strength temper.
- <u>H Temper</u> (Material Strain-hardened): Cold work that follows the annealing or simultaneously with partial annealing or consolidation.
- <u>W Temper</u> (Solution heat treated of the material): Unsteady temper, where the ageing time is only indicated.
- <u>T Temper</u> (Material treated in order to produce stable tempers (not H, F, O))**:** Solution heat treatment followed by ageing at room or medium temperatures (strain hardening may be provided) Further subdivisions are the following:
  - T1 refers to cooling from an elevated temperature that is followed by a kind of shaping process ending with natural ageing.
  - T2 refers to cooling from an elevated temperature followed by shaping process, cold working and natural ageing.
  - T3 indicates solution heat treatment, then cold working and naturally ageing
  - T4 consist of solution heat treatment and natural ageing
  - T5 refers to cooling from elevated temperature followed by shaping process and artificial ageing.
  - T6 indicates solution heat treatment and artificially ageing
  - T8 refers to solution heat treatment followed by cold working ending with and the artificial ageing.
  - T9 consist of solution heat treatment, artificial ageing and finally cold working
  - T10 indicates cooling from elevated temperature, some kind of shaping process followed by cold working and finally artificial ageing [3].

2.4   7005 and 7020 alloys

As stated earlier, 7005 alloy is an aluminum alloy used for bicycle frames; Because of its weldability, it doesn't require expensive heat treatment but it's quite hard to shape creating manufacturing difficulties. It's Ultimate Tensile Strength is 350MPa, Yield Strength 290MPa and density 2.78g/cm³ [6].

The 7020-alloy has the ability of natural age hardening; therefore, it recovers properties in the heat affected zone after the welding [7]. It has Ultimate Tensile Strength of 350 Mpa, a Yield Strength of 280 Mpa and a density of 2.78g/cm³, similar to 7005. Both belong to 7xxx series, that can harden throw precipitation [1].

The chemical composition of the two alloys is displayed in Table 2

Table 2: Chemical composition of 7005 and 7020 alloys (%wt.).

Sample	Al	Zn	Mg	Cr	Cu	Fe	Mn	Si	Ti	Zr
7005	91-95%	4,5%	1,4%	0,13%	<0,1%	<0,4%	0,45%	<0,35%	0,03%	0,14%
7020	91-95%	4,5%	1,2%	0,23%	0,2%	0,4%	0,30%	0,35%	0,03%	0,12%

2.5   Strengthening mechanisms of aluminum alloys.

The strenghtening mechanisms of aluminum alloys occures due to the creation of some effective obstacles in the movement of mobile dislocations. Those obstacles can be grain boundaries, microstructural inhomogeneities, solute atoms, phase interfaces, and dispersed secondary precipitates. Based on the nature of impediments and their interaction with dislocations, the main strengthening mechanisms in aluminum-based alloys include [8]:

- Grain size strengthening
- Solid solution hardening,
- Dislocation strengthening
- Precipitation hardening

In grain size strengthening mechanism, we study the connection between the grain size and the mechanical properties . The grain boundaries increase the yield stress by opperating as obstacles to the dislocation movement. Hall Petch equation describes the relation between yield stress and the size of the grains [9].

$$\sigma_y = \sigma_0 + \frac{k_y}{\sqrt{d}}$$

In the above equation σ_y refers to the yield stress, while σ_0 represents a materials constant that indicates the starting stress of the dislocation movement. Strengthening coefficient is represented by K_y and the average grain diameter by d. The Hall Petch equation is empirical and fits the experimental data [10].

The grain refinement and more special the microstructuring can signifficantly improve the mechanical strength of aluminum alloys [8].

The solid solution hardening mechanism refers to an increase in the critical resolved shear stress as a result of introducing a second element. This enhancement strongly depends on some determining parameters such as solute elements, their distribution, concentration, and temperature [11].

The dislocation strengthening mechanism introducs a high density of mobile dislocations into aluminum matrix that rises the hardness and the mechanical strength. These extra dislocations are coming from plastic deformation and create compact networks which are

called cell structures. Aluminum alloys that are plasticly deformed often present this mechanism, where the application of high strains in the material cause the shrink of the grains [12].

The precipitation hardening mechanism occurs mostly in ageable aluminum alloys such as 7005 and 7020 alloys of the 7xxx Al-Mg-Zn series. Mainly the only requirement for precipitation hardening is a graduate drop in solid solution limit of an alloy while the temperature falls. In the above alloys , the strengthening effect is simulated by the interaction of the dislocations with the particles [13]. In our work the implications of the basic alloying elements (Mg and Zn) is that they are considerably enhancing the mechanical strength. However, they can cause stress corrosion in the alloy. The main properties of the alloy are high strength, essential sensitivity to stress corrosion and over-ageing at high temperatures. The most common equilibrium compounds in these alloys include $MgZn_2$, Mg_5Al_8, Mg_2Zn_{11} and $Mg_3Zn_3Al_2$ [8]. This kind of hardening will be studied more extensively in section 2.6 alongside with the ageing process which is a significant process of the precipitation.

2.6   Ageing in aluminum alloys

As mentioned above, the precipitation hardening is a main strengthening mechanism in which some customizable precipitates are scattered inside the metal matrix, blocking the gliding of the mobile dislocations and immobilizing them. The precipitation hardening occurs in some subsequent steps:

- Solution heat treatment at the appropriate temperature .
- Rapid cooling by quenching into water or other cold mean.
- Ageing heat treatment for an enough time to form second phase precipitates inside the initial matrix.

In the first step there is homogenization of matrix and redistribution of solute atoms inside it. In the second step suppression in the instant formation of stable spredings occurs that maintains the super-saturation of the initial matrix. At last, the third heat treatment opens the way for the separation and the controlled growth of second phase precipitates from the matrix . This procedure happens by a nucleation and growth mechanism [14].

The age heat treatment occurs also in several susequent stages:

- The formation of clusters from solute atoms.
- The formation of Guiniere-Preston zones(GP zones).
- The formation and development of metastable phases.
- The formation of equilibrium phases from the metastable phases.

The main characteristics of formed precipitates can affect the mechanical performance of ageable aluminum alloys, significantly. These characteristics can be some geometrical specifications, the chemical composition, and distribution of precipitates. The above

19

parameters can be managed throw the chemical composition and ageing heat treatment of the alloy [15]. It is usual that some alloying elements are used to create the favorable precipitates in aluminum alloys such as Mg, Zn, Cu, Si, and Li. The simultaneous use of these elements provides more strengthening. As stated in previous sections, aluminum alloys can be categorized into heat treatable and non-heat treatable. The heat treatable or ageable Al alloys include the Al-Cu, Al-Cu-Mg, Al-Mg-Zn, Al-Cu-Li, Al-Mg-Si, Al-Zn-Mg-Cu and Al-Li alloys [8].

Many sediments can be created depending on the main alloying elements and the thermal procedure that we apply during the ageing process. Secondary phases that are created, are presented in Table 3. Further precipitates can be also formed in Al alloys.

Table 3: The common precipitates in the main ageable aluminum alloys [15].

Al alloy Series	Main alloying elements	Precipitates
2xxx	Al, Cu, (Mg)	$GP \rightarrow \theta'' \rightarrow \theta'(CuAl_2)$
6xxx	Al, Mg, Si	$GP \rightarrow \beta'' \rightarrow \beta'(Mg_2Si)$
7xxx	Al, Zn, Mg	$GP \rightarrow \eta' \rightarrow \eta(MgZn_2)$
8xxx	Al, Li	$\delta'(Al_3Li) \rightarrow \delta(AlLi)$

2.7 Welding of Al-Mg-Zn system

The welding process is widely used for joining Al-Mg-Zn alloys as those has excellent weldability. During the welding process the materials are put alongside and melted in their common surface and after the solidification the joint that has performed is permanent. This process creates three zones in the metal. The first one consists of the base metal and is unaffected from the heat keeping its microstructure and abilities (Hardness, mechanical properties etc.). The second one is the heat affected zone, where the temperature of the metal has reached high enough values to change the microstructure and the mechanical properties. In this zone the temperature of the metal reaches values lower to the liquidus and causes precipitation. The last zone is the fusion zone that consist of the welded metal and the temperatures are above the liquidus. After the solidification the microstructure is totally different from the initial metal by developing casting form which reduces the mechanical properties significantly.

For the welding process there can be a variety of energy sources that can be used, such as gas flame, electric arc, laser friction, ultrasound and electron-beam.

The most commonly used arc welding types for aluminum alloys are the following:

- Gas Metal Arc Welding (GMAW)
- Gas tungsten arc welding (GTAW)

Gas metal arc welding (GMAW), known also as metal inert gas or MIG welding, uses an inert gas for protection and a consumable electrode that creates an electric arc which provides the heat [16].

Gas tungsten arc welding (GTAW), also known as tungsten inert gas (TIG) welding, is type of welding that uses a non-consumable wolfram electrode and an inert gas for protection. This process can be both automatic and semiautomatic and has a continuous wire supply [16].

The welding method that is used in a joint, alongside with the properties of the welding such as the diameter of the wire, electric current, voltage, inert gas and welding speed define the quality of the welding and therefore the microstructure of the materials.

2.8   Thermodynamic description of Al-Mg-Zn alloys

Although 7xxx series aluminum alloys consist of Al and Zn, some other elements such as Mg, Cu and Zr can be added to change the mechanical response of these alloys through the formation of favorable precipitates [17-20].

These alloys can evolve precipitates as stated earlier during the ageing and as a rule, the type, density, and geometrical characteristics of those precipitates specify the mechanical properties of the alloys [21, 22]. The most common precipitates are $MgZn_2$ and Al_3Zr, however other compounds can form depending on the alloying elements and applied thermal procedures [8].

During the ageing progress the following precipitates can grow [23]:

- GP zones
- η' phase
- η phase

(a)   (b)
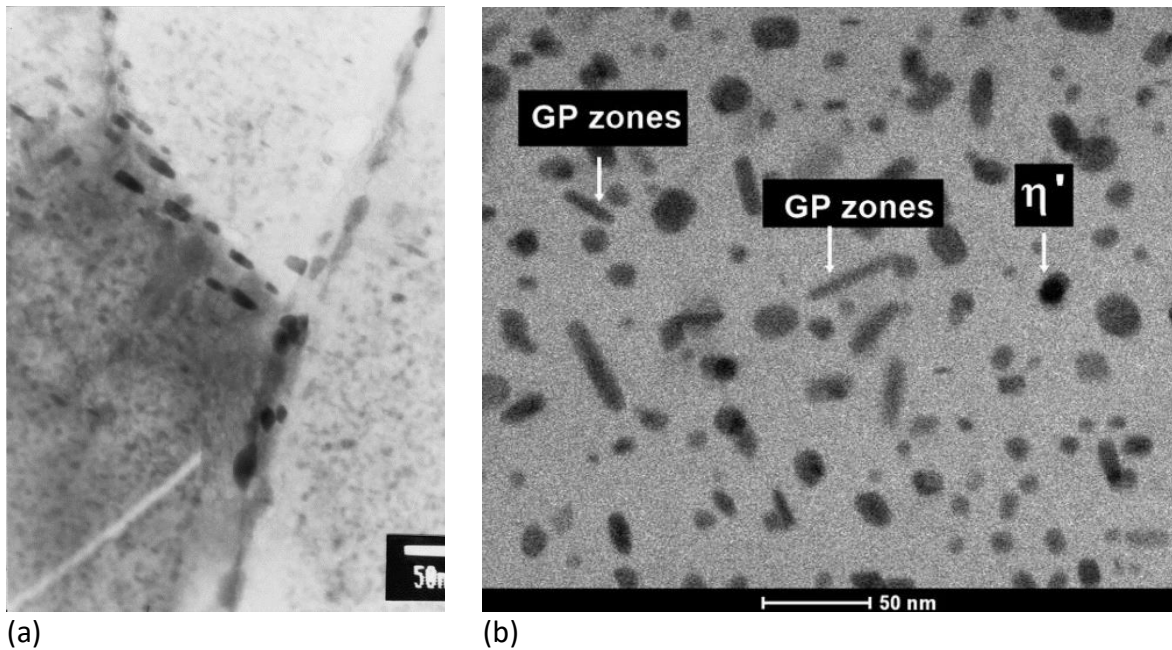
Figure 2: a)Bright field TEM image of the η-MgZn2 equilibrium phase precipitated on the grain boundary of an aluminum matrix, b) Bright field TEM showing a fine distribution of precipitates and GP-2 zones inside aluminum matrix [23].

GP zones basically cause precipitation hardening in aged 7xxx aluminum alloys while their structure is hexagonal grid and becomes consistent with the matrix. Their size is about a few nanometers in diameter.GP zones are formed in two categories the GP-1 and GP-2 zones and are formed in the early stages of the precipitation. The GP-1 zones appear in low temperatures, from room temperature to approximately 150°C and are independent of the solution treatment or quenching temperature. The GP-2 zones form in quenching from high temperatures over 450 C and at ageing above 70°C. During the ageing, the GP-zones, convert to $\acute{\eta}$ phase which is a metastable and semi-consistent intermediate phase. The ageing time and temperature is highly affected by the size of the $\acute{\eta}$ precipitates. In continuous aging at temperature above of 150 C, the $\acute{\eta}$ precipitates form in both parallel and vertical directions of the [24] aluminum planes, reducing the consistency with the matrix and transforming into the non-consistent η phase [25]. This η phase has also a hexagonal crystallographic structure. Depending on the crystallographic orientation relationships between aluminum and η phase, there are 11 types of η phase, known as η_1- η_{11} and the most significant of those is MgZn$_2$ [15].

The transformation of the microstructure can be explained by the following scheme:

Solid solution(a)→ GP zones→η'→η→MgZn$_2$ [26]

Studies have shown that there is a connection between Zn : Mg ratio and the precipitation kinetics which affects the mechanical properties of the alloy [27].

22

In order to predict the relation between the precipitation and the ageing of 7xxx series aluminum alloys, we must find a connection between the ageing duration and the grid parameter of the matrix. Results of studies have shown the inverse relationship between the hardness and the matrix parameter for every condition. Therefore, the maximum hardness corresponds with the minimum matrix parameter [28].

The Al-Mg-Zn alloys phase diagram is basic for both alloys we have received (7005 and 7020). For the most probable of the Al-Zn phase diagrams, its ternary system has in equilibrium with the Al-phase, the following phases: Al_2Mgs, $Al_2Mg_3Zn_3$, $MgZn_2$, Mg_2Zn_{11}, and Zn.

The Al_2Mg_5 phase dissolves up to 10% Zn. The $MgZn_2$ has hexagonal structure as stated earlier and contains about 84% Zn. The Mg_2Zn_{11} binary phase contains 6,3% Mg and has cubic structure. The ternary phase compound $Al_2Mg_3Zn_3$, contains 20-35% Mg and 22-65% Zn and can be found also as $(AlZn)_{49}Mg_{32}$. It has also cubic structure and is usually designated as T phase. Lastly, the Zn phase is a solid solution of Al and Mg in Zn. The solubility of Mg is up to 0.1% and of Al about 0.5%.

The phase diagrams of the Al-Mg-Zn system, as well as the liquidus, solidus and solvus isotherms, are presented in the figure below [29].
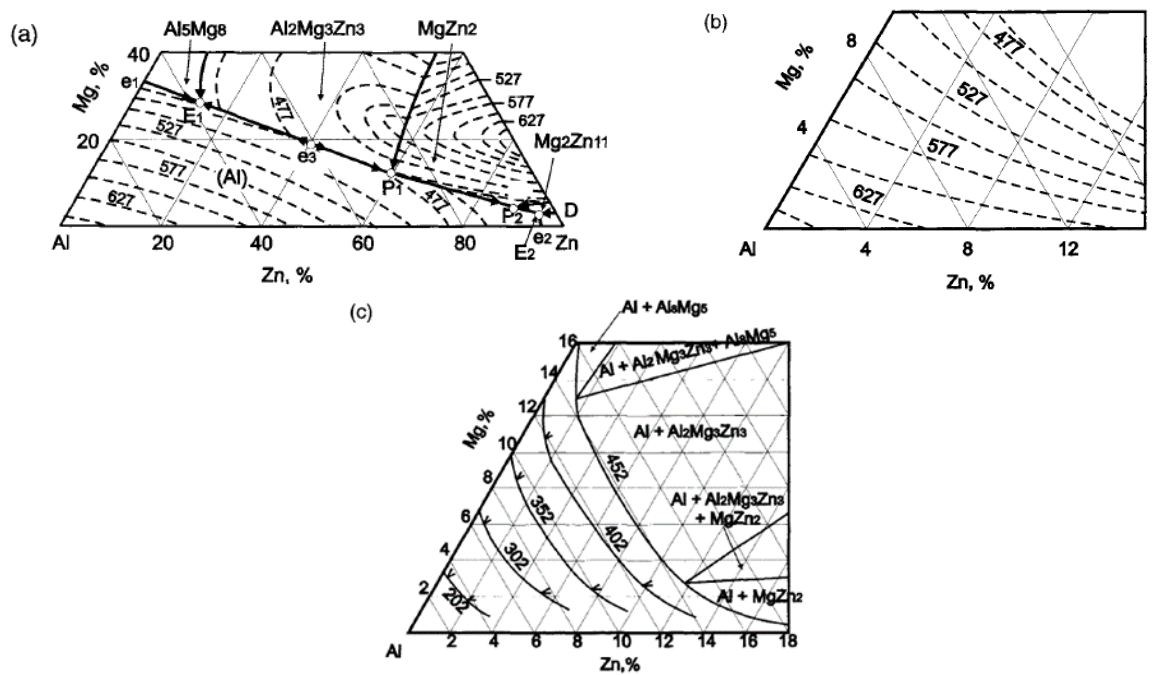
Figure 3: Phase diagram of Al-Mg-Zn alloys a) liquidus surface and isotherms b) solidus isotherms c) solvus isotherms [29].

23

3 Experimental procedure

3.1 Materials Studied

As stated earlier, the focus of this research was aluminum alloys that belong to the 7xxx alloy series, more accurately, alloys 7005 and 7020. The 7005-alloy was obtained in 2 cylindrical pipes with thickness 3.2mm. Each of the pipes was obtained from a different supplier and with different initial aging treatments. The first one was received in the T6 heat treatment and the second one with the T1 heat treatment. T1 heat treatment is the aging process, where the alloy is cooledT from an elevated temperature, followed by a kind of shaping process and then naturally aged. T6 refers to solution heat treatment and artificially aging. The 7020 alloy was obtained in a welded plate form and it was initially aged through T6 heat treatment.

The chemical composition of both 7xxx alloys is displayed below in Table 4, while in Table 5 the heat treatment of the two 7xxx aluminum alloys is presented.

Table 4: Chemical composition of the 7xxx aluminum alloys (%wt.).

Sample	Al	Zn	Mg	Cr	Cu	Fe	Mn	Si	Ti	Zr
7005	91-95%	4,5%	1,4%	0,13%	<0,1%	<0,4%	0,45%	<0,35%	0,03%	0,14%
7020	91-95%	4,5%	1,2%	0,23%	0,2%	0,4%	0,30%	0,35%	0,03%	0,12%

Table 5: Heat treatment of the two 7xxx aluminum alloys.

Material	Temperature Dissolution	Heat treatment
7020	470°C	T6
7005	400°C	T1 T6

In Figure 4 a photograph of the two 7005 pipes is presented.
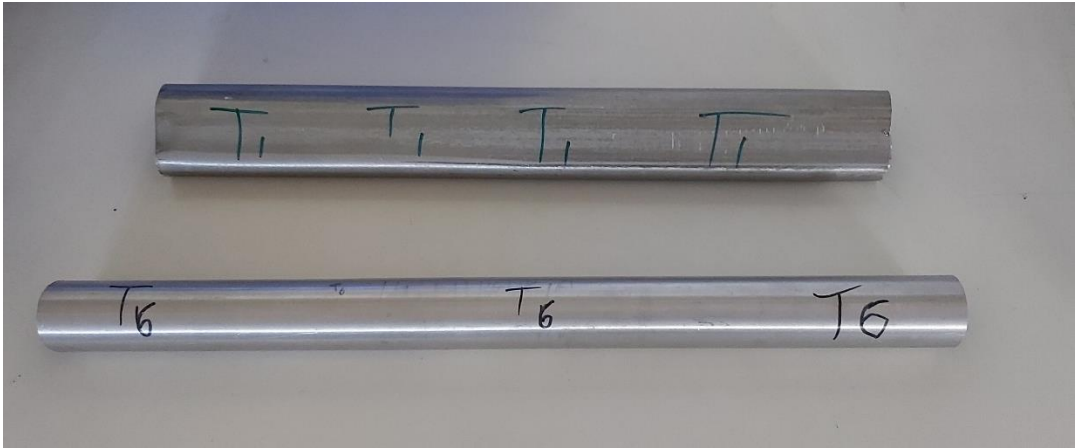
Figure 4: The two 7005-alloy pipes with T1 and T6 heat treatment.

In Figure 5 a photograph of the welded 7020 plate is presented.
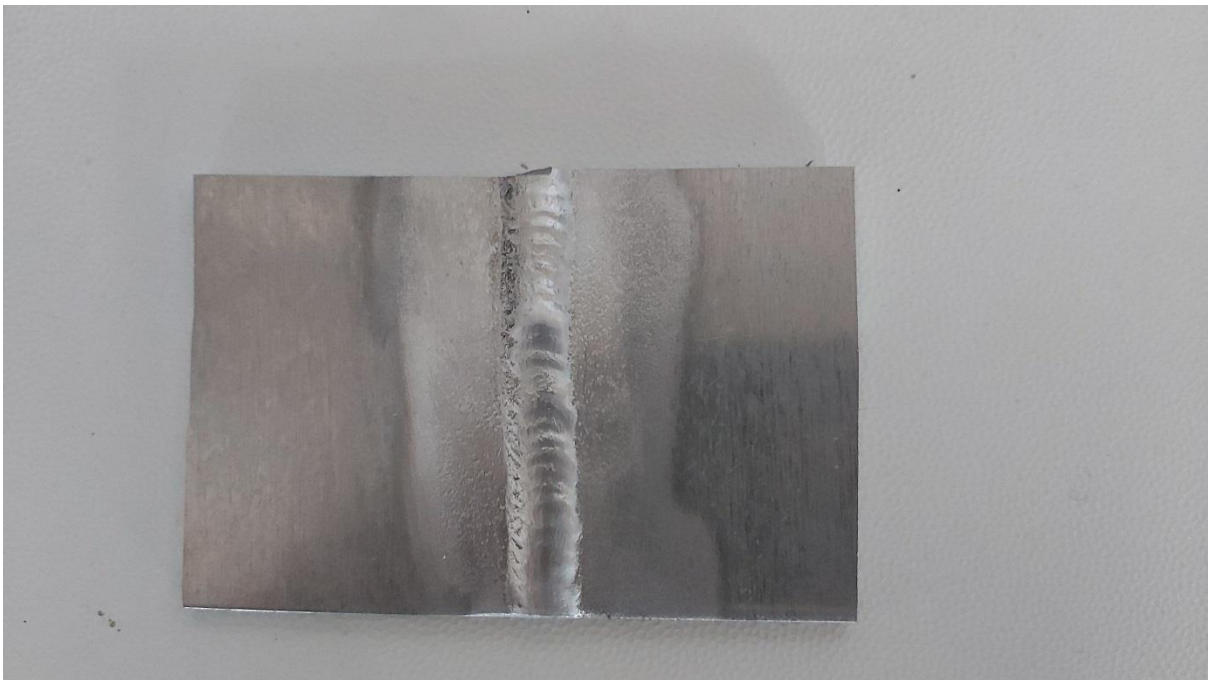
Figure 5: The 7020 Al alloy welded plate.

The two pipes of 7005 were cut to appropriate size specimen and given to Lazaro Bros Sheet Metal Work for the welding process. The 7020 alloy plate was provided with the weld.

3.2   Welding of 7005 T1-T6 specimens

For the weld of 7005-T1 and 7005-T6 alloys, three weld types were performed.

- T1-T1 weld
- T6-T6 weld
- T1-T6 weld

For both T1-T1 and T6-T6 welds, two cylindrical pipes where joint together vertically, as it is shown below in Figure 6 for T1-T1 pipes. The welding was performed with the GMAW welding process.

Figure 6: Photograph of the welded T1-T1 pipes.

On the other hand, the T1-T6 GMAW welding was formed by using two quarter-cylinder plates horizontally, as the following picture presents.
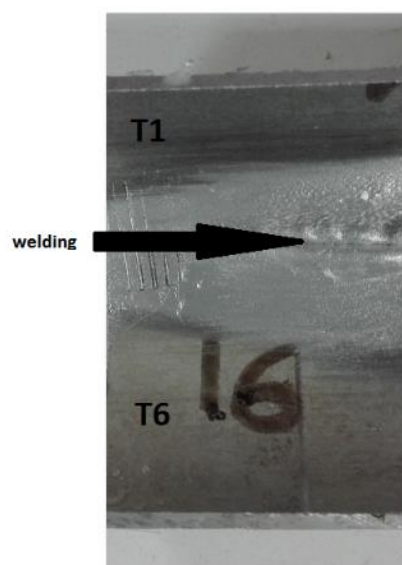
Figure 7: Photograph of the welded T1-T6 pipes.

There are two kinds of welding processes that were suggested for the joint of 7005 alloys: GTAW and GMAW. The properties of each welding processes are presented in Table 6 and Table 7, while the composition of the proposed wire is presented in

Table 8. The weldings for the present experiment were all performed under GMAW process.

Table 6: Welding properties of GTAW (TIG) [23].

Welding type	GTAW
Filler alloy	OK Tigrod 5356
Welding current	AC (130-150 A)
Filler Material diameter	1.5-2.4 mm
Welding voltage	50-100 V
Welding speed	4-6(mm/sec)
Argon gas flow	8-10 (L/min)

Table 7: Welding properties of GMAW (MIG) [27].

Welding type	GMAW
Filler alloy	ER 5356
Welding current	AC (160-180 A)
Welding voltage	18-22 V
Wire feed rate	8.6-9 (m/min)
Argon gas flow	15-18 (L/min)

Table 8: Composition of the wire ER 5356.

Si	Mn	Cr	Cu	Ti	Zn	Fe	Mg
<0.25%	0.15%	0.13%	<0.05%	0.11	<0.10%	<0.40%	5.0%

3.3 Heat treatment -ageing experiments

3.3.1 Post Weld Heat Treatment

The post weld heat treatment was performed by extracting specimens from the welded material and exposing them to several heat treatments.

- Room Temperature for 1 year
- Heating for 12 hours at 120°C.
- Heating ageing for 24 hours at 120°C.
- Heating ageing for 42 hours at 120°C.
- Step heating for8 hours at 100°C, followed by 24hours at 150°.C

3.3.2 Post Weld Heat Treatment Simulation of base metal

After cutting the 7005 welded specimens were post weld heat treated at 120°C for different times and then cooled to room temperature. The post weld heat treatment removal

times were 30 minutes, 1h, 2h, 4h, 6h, 8h, 10h, 12h, 24h and 42h. Furthermore, the weldings were heated at 120 °C for 12, 24 and 42 hours in order to restore the microhardness of the heat affected zone back to the base metal's. Finally, there was a heat affected zone simulation were samples of the as received material were heated for 5 minutes in temperatures between 150 and 550 °C and then aged in 120° for 24 hours

3.3.3   HAZ simulation

The HAZ simulation was performed by extracting small specimens of the material and exposing them to several temperatures. The lowest temperature was 150°C and the highest 550°C, near to the liquidus temperature (643°C). The temperature each sample was exposed to, defines the point of the heat affected zone that it belongs.

3.3.4   Post Weld HAZ simulation

After the simulation of the heat affected zone, the specimens were subjected to an heating treatment in order to equalize the values of the microhardness.

- Heating for 24 hours at 120°C.

3.4   Specimens preparation - Cutting

Parts of the welded pipes, as well as the 7020 plate, were cut for further investigation with optical microscopy and microhardness measurements (microhardness profiles). In Figure 8 an illustration of the cutting process of the welded T1-T1 and T6-T6 cylindrical pipes is presented. The resulting specimens were prepared for standard metallographic analysis, as described in the following sections.

Furthermore, the base material of both pipes was cut into smaller specimens, in order to be used in heat treatment experiments.

Two series of heat treatment experiments were conducted. Experiments simulating the microstructural evolution of the Heat Affected Zone, as well as experiments to determine the best suited post weld heat treatment.

Figure 8: Cutting sequence of the 7005 T1-T1 and T6-T6 welded pipes.

The welded T1-T6 plate was cut with the same way that the 7020 plate was cut, vertical to the welding line as shown below (Figure 9).

<table>
<tr><td>(a)</td><td>(b)</td></tr>
</table>
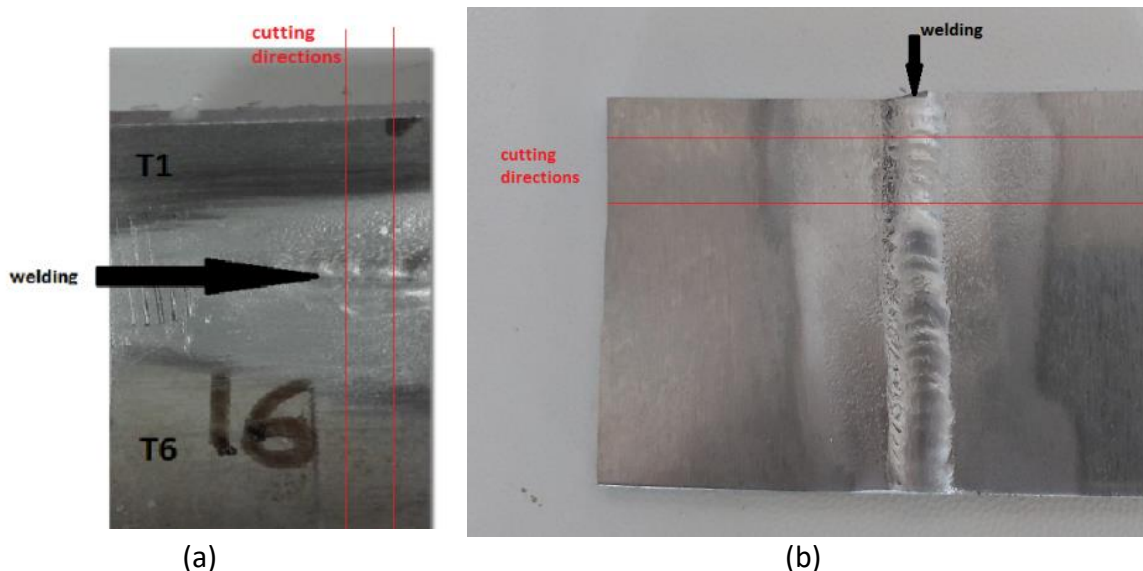
Figure 9: Cutting directions of a) 7005 T1-T6 MIG welding b) 7020 MIG welded plate.

3.5 Metallographic analysis and Microhardness tests

All the specimens were placed in epoxy resin for easy handling (Figure 10). The resin fills the pores, voids and surface abnormalities of the specimen. The surface planes under observation were the rolling direction and the longitudinal surface. Next the samples were initially grinded on SiC abrasive wheels. The sizes of grains were 80, 120, 180,220,300, 500, 800, 1000, 2000 grid. Polishing of the specimens followed on special disks with diamond paste of 3μm and 1μm grain size respectively. The last stage of preparation was polishing with Al_2O_3 particles of 0,3μm and 0,05 diameter respectively. After that, the surface was chemically etched with Keller's reagent. This reagent has a chemical composition of: *2,5 ml HNO₃, 1,5 ml HCl, 1,0 ml HF and 95,0 ml H₂O*. The time of exposure in Keller's was about 20 seconds. Finally, the specimens were washed with distilled water and alcohol and dried in a purge of warm air. Subsequently, these were ready for observation in the optical microscope and for microhardness tests.

Figure 10: Specimen surrounded by epoxy resin.

3.5.1 Metallography

The observation of the samples was held in the scales of 50x, 100x, 200x and 500x magnification in order to watch and photograph the microstructure (grain boundaries and size). An optical microscope was used with a camera adapted on which captured the pictures

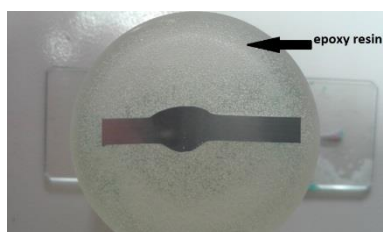in the following sections. For the measurements of the grain size and the calibration of the images, Adobe Photoshop and Image Pro Plus were used. The pictures of the metallographic analysis that took place are presented above as well as the average grain size of the samples.

3.5.2 Microhardness measurements

Following the metallographic analysis, the microhardness of all specimens was measured. In general, hardness is defined as the property of a material to resist to the penetration of another, harder material. Firstly, polishing is required, in order to create a new mirror like surface, quitted from previous chemical etchings. A Woolpert Vickers microhardness tester was used. For the measurements a diamond penetrator with regular square pyramid shape was used. The penetrator leaves on the specimen surface a rhombical trace with d1 and d2 diagonals. Micro hardness tests were carried out with a 200gram (0.2 kg) load. The two diagonals of the rhomb are measured giving the final value of the micro hardness in Vickers scale (HV) according to the following formula: $HV = F/A = 1.854*F/d^2$, where F is the imposed load, A the trace surface area and d = (d1 + d2) / 2 (average diagonal value.

4 Results

4.1 Metallographic analysis of 7005-T1 Aluminum alloy – Base metal.

In this section we observe the metallography of the 7005-T1 aluminum alloy as received.

As we can see at the following figures (Figure 11-Figure 13) there is a significant difference in the grain size between the longitudinal and transverse direction. This is the result of the machining progress called extrusion where the material is pushed through a die of the desired geometry. This pull is responsible for the elongated grains Also, as at is clearest in the Figure 11 the grain size in the edge of the specimens is smaller than in the center of them. The average grain size of the longitudinal direction is approximately 520 µm in the center and 200 µm in the surface, as well as in the transverse, the centrical grains have a mean diameter of 150 µm and surface of 50 µm. The size difference between the grains of the alloy in the two directions lies in the manufacturing process of the material, in this case is extrusion, which elongates the grains in its direction.

(a)   (b)

Figure 11: Micrograph of Al 7005 T1 as received under 50x magnification at a) longitudinal direction and b) transverse direction.

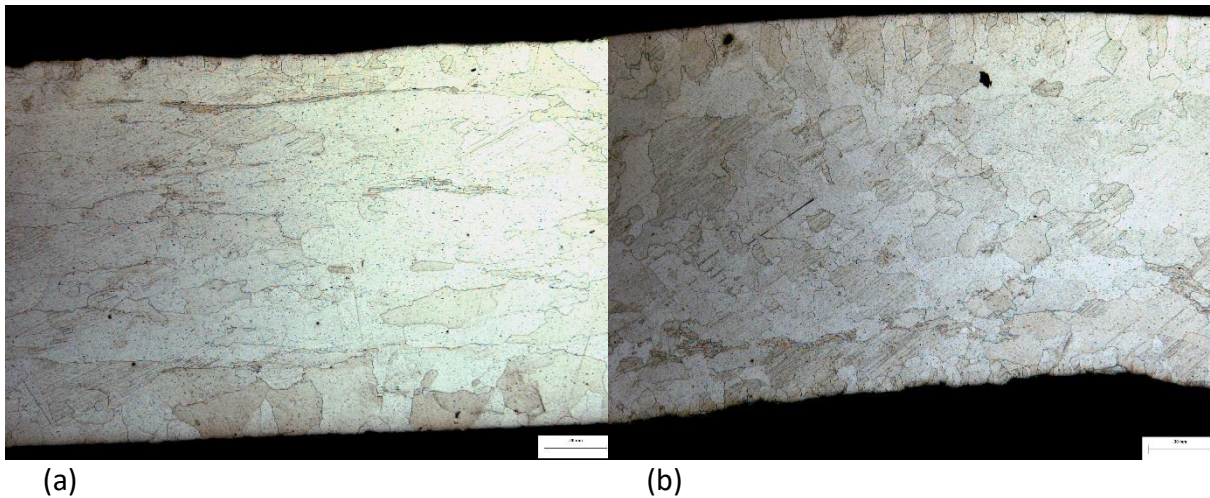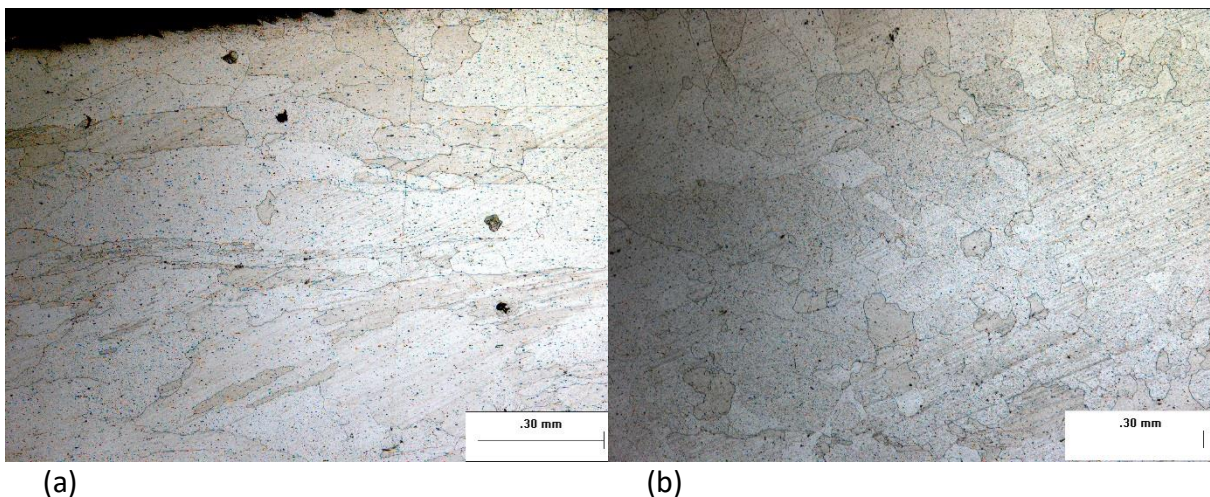(a)   (b)

Figure 12: Micrograph of Al 7005 T1 as received under 100x magnification at a) longitudinal direction and b) transverse direction

(a)   (b)

Figure 13: Micrograph of Al 7005 T1 as received under 200x magnification at a) longitudinal direction and b) transverse direction

4.2   Metallographic analysis 7005-T6 Aluminum alloy - Base metal.

As in the previous 7005-T1 alloy, the T6 one shows significant difference between the grain size in the longitudinal and the transverse direction, due to the extrusion progress (Figure 14-Figure 16). More specific in the longitudinal direction the grain size is about 150-450 μm and in the transverse 30-170 μm. However, there isn't any difference in the surface grains and the central ones.

(a)   (b)

Figure 14: Micrograph of 7005-T6 specimen as received under 50x magnification at a) longitudinal direction and b) transverse direction

32

(a)   (b)

Figure 15: Micrograph of 7005-T6 specimen as received under 100x magnification at a) longitudinal direction and b) transverse direction
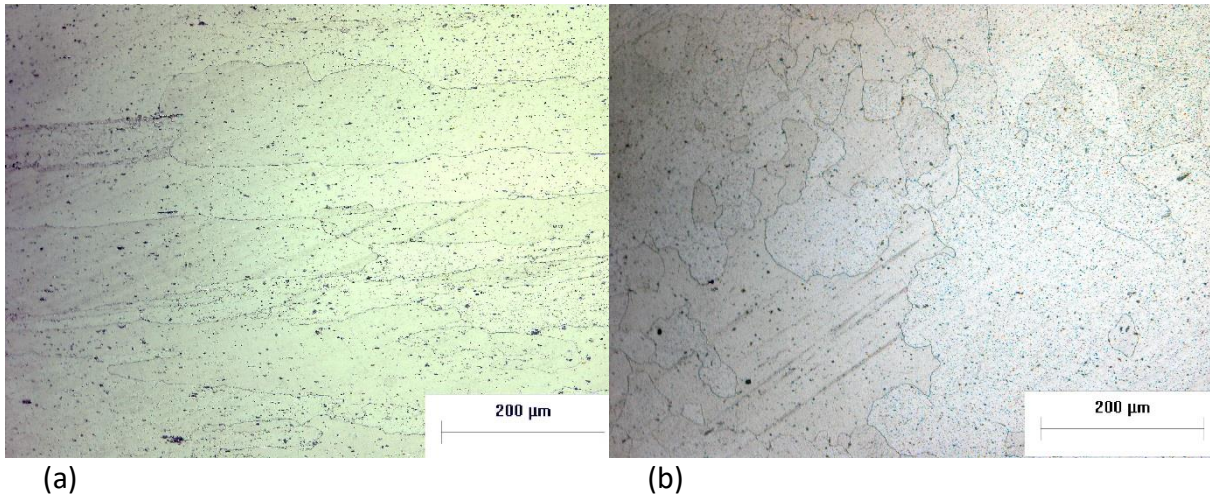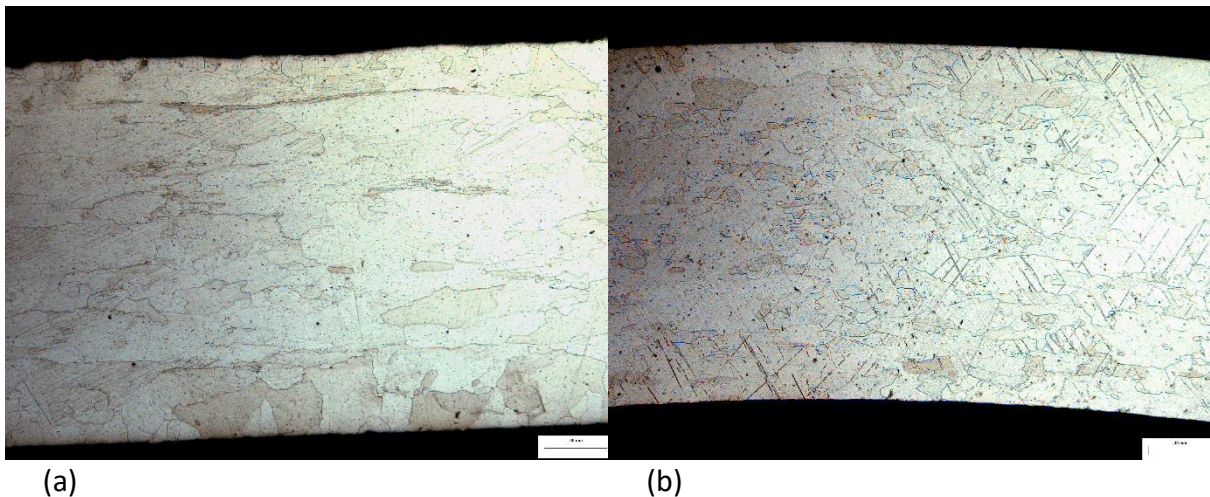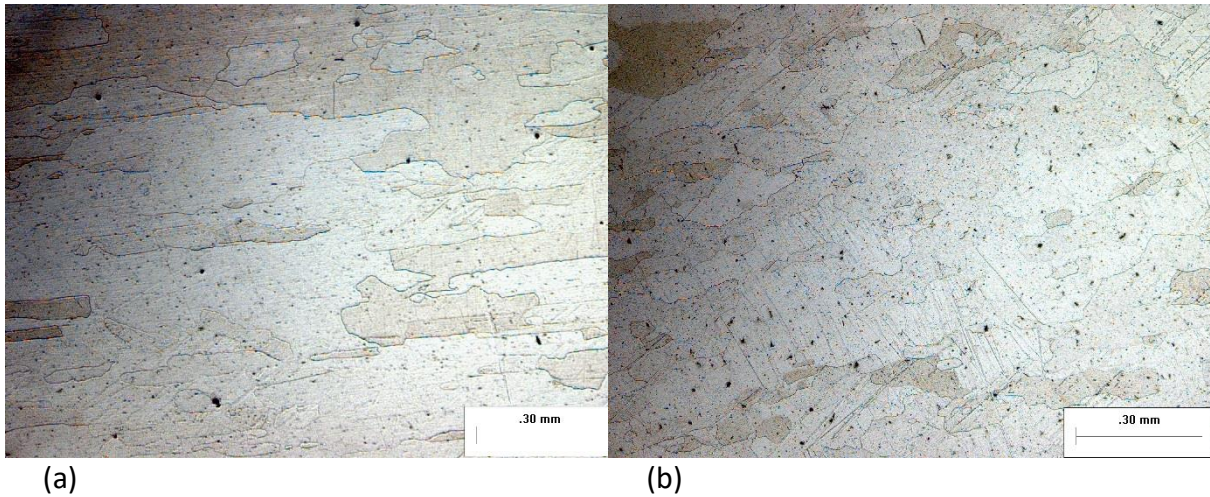

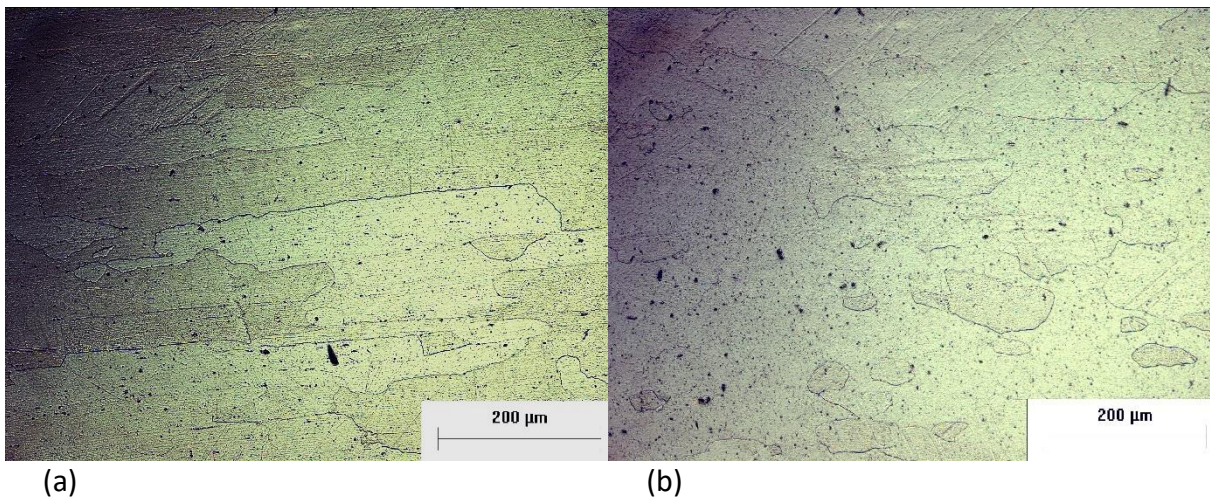(a)   (b)

Figure 16: Micrograph of 7005-T6 specimen as received under 200x magnification at a) longitudinal direction and b) transverse direction

4.3 Metallographic analysis of 7005 alloy welds

4.3.1 Welding of 7005- T1 alloy with 7005-T6- alloy (MIG).

In this section we present the 7005-T1-T6 welding. At first, the welding plate is presented as received from the workshop (Figure 17). The welding type that was performed was MIG and the properties were presented in section 3.2. Subsequently, it was cut in small samples as shown in the Figure 18 ,vertical to the welding direction. After that, the photos of the microstructure of the weld are presented. The Figure 19 shows the studied areas in the following metallographic analysis. The areas b1 and b2 refer to the base metal of the T1-side of the weld. The Haz1 represents the Heat affected zone of the T1. In the same way b3 and b4 represent the base metal of the T6 side and the Haz2 its heat affected zone. The metallographic analysis of those areas is presented in the Figure 20-Figure 26.

33
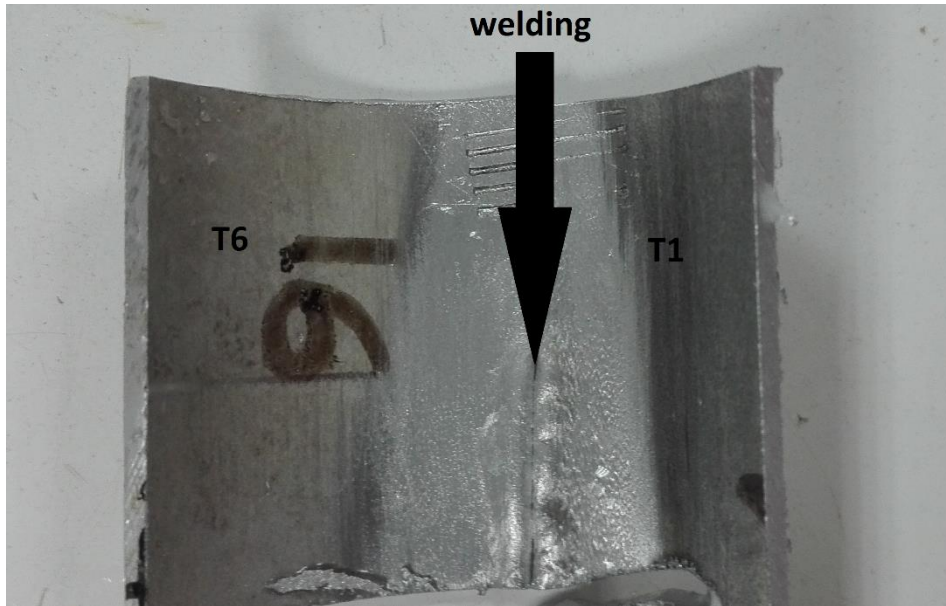
Figure 17: Image of the MIG T1-T6 welding. 7005-T6 alloy in the left is joint alongside with 7005-T1 alloy in the right.

Figure 18: Samples of the T1-T6 welding. Half-cylindrical samples created by cutting the above plate vertically to the welding.

Figure 19: Studied areas of the welding between 7005-T1 and 7005-T6 samples. The left side consist of 7005-T1 material and the right side of 7005-T6.

(a)

(b)

Figure 20: Micrograph of B1 area consisting of base metal at magnification of a) 50x b) 200x

(a)

(b)

Figure 21: Micrograph of B2 area consisting of base metal at magnification of a)50x b)200x

(a)	(b)

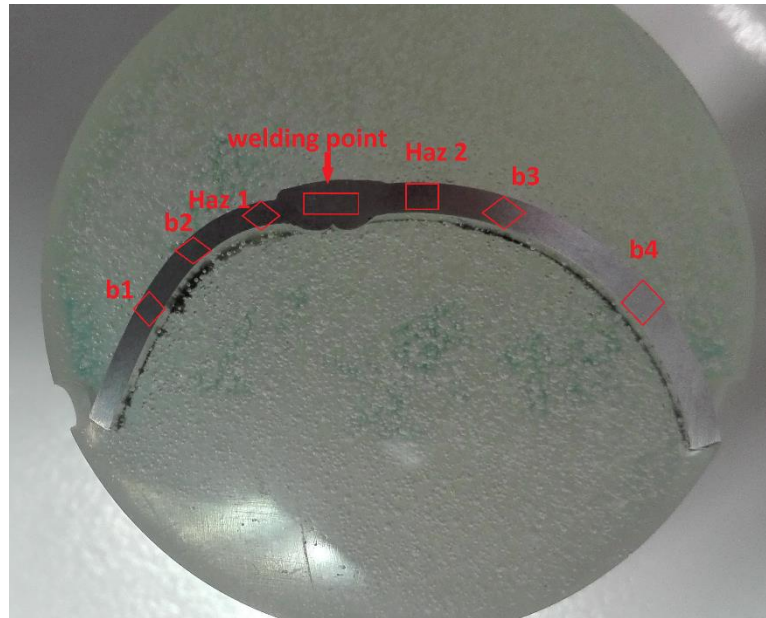Figure 22: Micrograph of HAZ1 area consisting of heat affected zonel at magnification of a)50x b)200x

(a)	(b)

Figure 23: Micrograph of WP area consisting of welded metal at magnification of a)50x b)200x

(a)	(b)

Figure 24: Micrograph of HAZ_2 area consisting of heat affected zone at magnification of a)50x b)200x

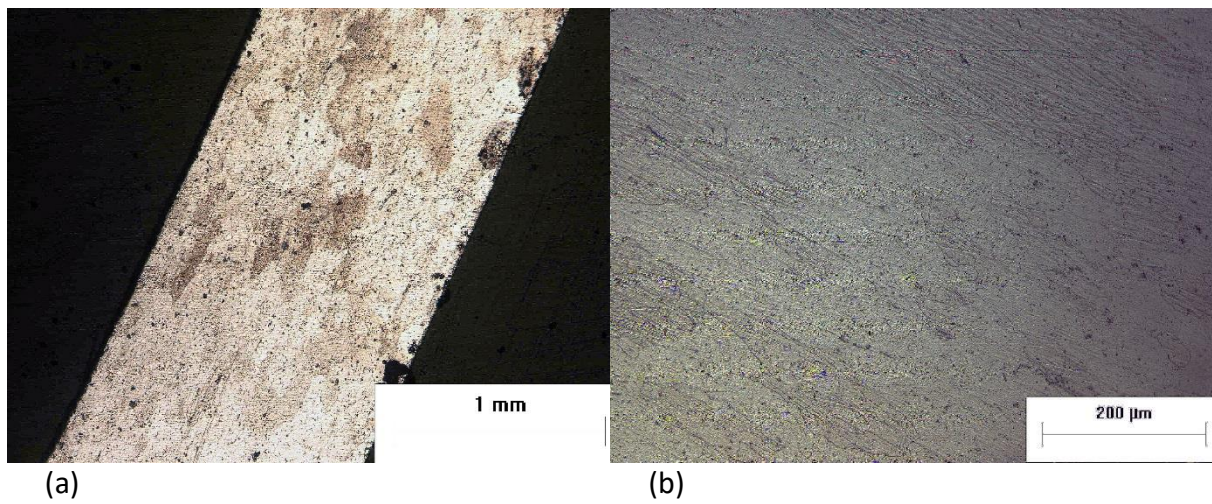(a)   (b)
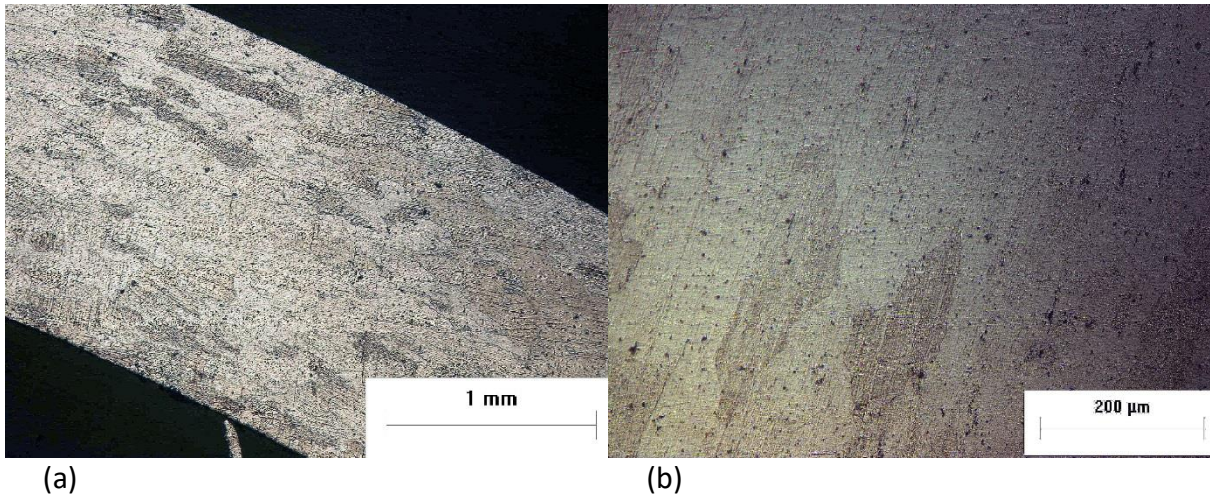
Figure 25: Micrograph of B_3 area consisting of base metal at magnification of a)50x b)200x

(a)   (b)
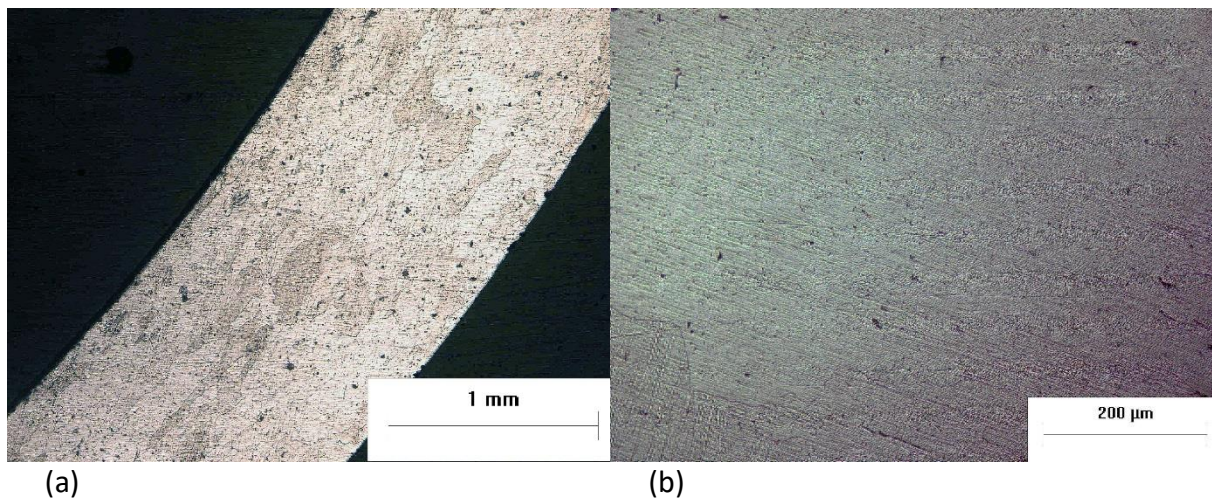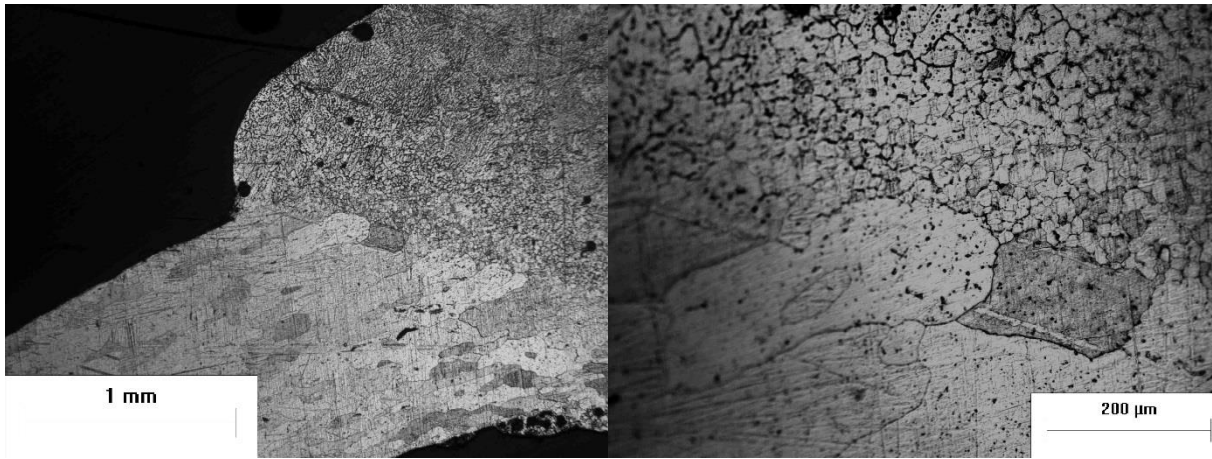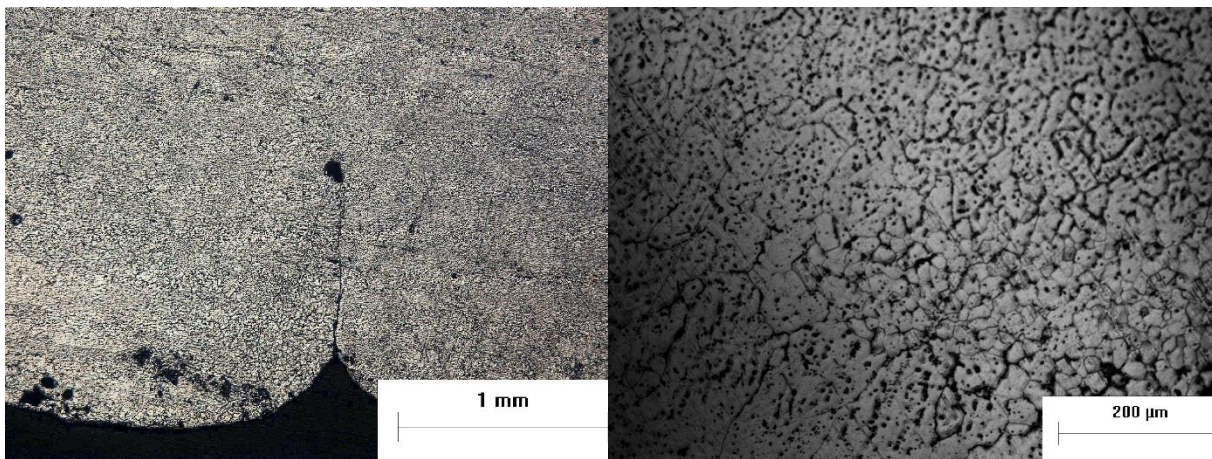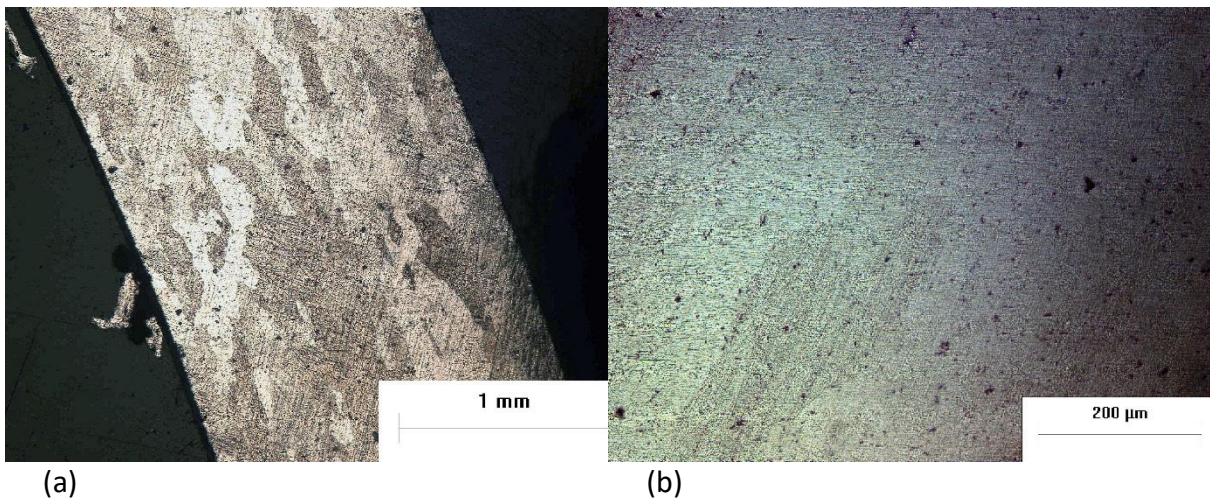
Figure 26: Micrograph of B_4 area consisting of base metal at magnification of a)50x b)200x

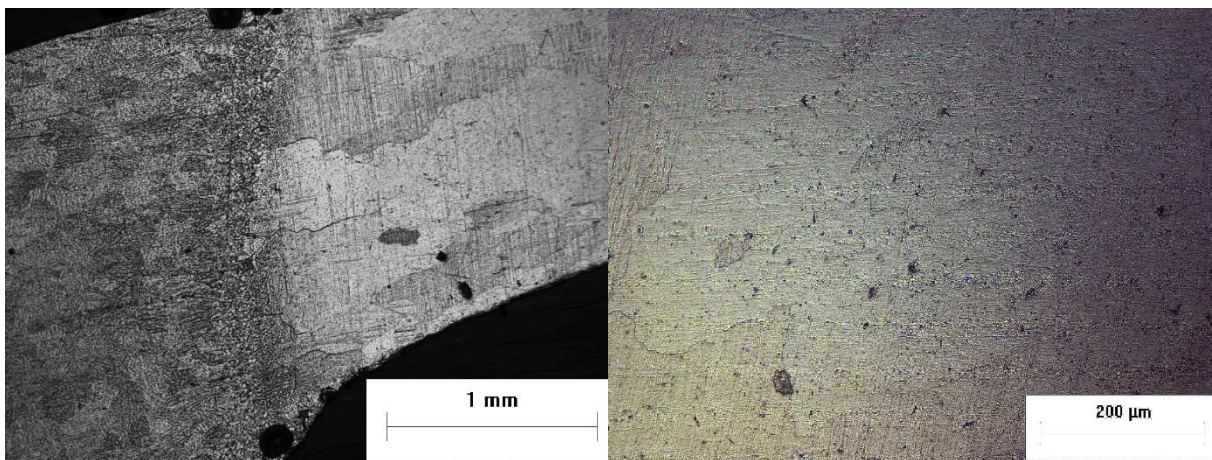As it is obvious in the figures above, the base metal has a microstructure of big grains as it is not affected by the heat input of the weld and as a result it constitutes as received metal. In the heat affected zone (HAZ) the size of the grains is similar to the base metal as the heat from the welding doesn't affect significantly the grains of the alloy. As stated earlier, the way to separate the HAZ from the base metal lies in the microhardness tests that are presented in the following sections. Lastly, at the weld point, the metal has melted acquiring casting structure with columnar forms such as dendrites.

The measurement of the grain size of the above welding is presented in the Table 9.

Table 9: Average gran size in the studied areas

Area	Average grain size (μm)
Base Metal	50-150
HAZ	80-150
Welding Point1	Casting structure

4.3.2 Welding of 7005- T1 alloy with 7005-T1- alloy (MIG).

The welding of the 7005-T1 alloy was performed by joining the two pipes vertically with MIG progress as presented in Figure 27. The welding properties are also presented in section 3.2.

Figure 27: Macrograph of MIG welding between the 7005-T1 pipes.

In order to perform the metallographic analysis, we needed to cut the welding in smaller samples as show in the following figure.

| a | b | c | d | e |
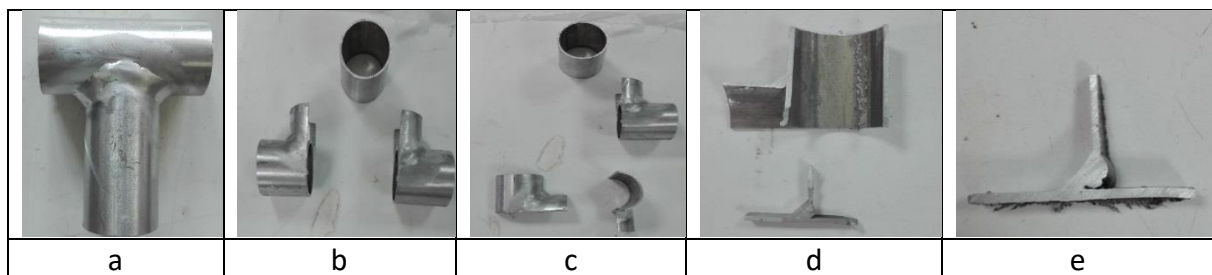
Figure 28: Cutting process of the 7005-t1 welding a) isolation of the welding b) cut the welding in two samples to reveal the inside surface c) Quarter cut the previous samples in order to make it easier to handle d) final cut before boxing e) final sample isolated.

After the boxing, grinding, polishing, and chemically etching processes which have been described previously, the metallographic analysis is ready to take place. The studied areas of the welding are presented in the Figure 29.

Figure 29: Studied areas of the 7005-T1 welding

The microstructure of the above areas is presented in the Figure 30-Figure 34. All the photos are in 50x magnification.

(a)   (b)

Figure 30: Micrograph of base metal areas in **b**-direction under 50x magnification a) b_1 area b) b_2 area:

(a)   (b)

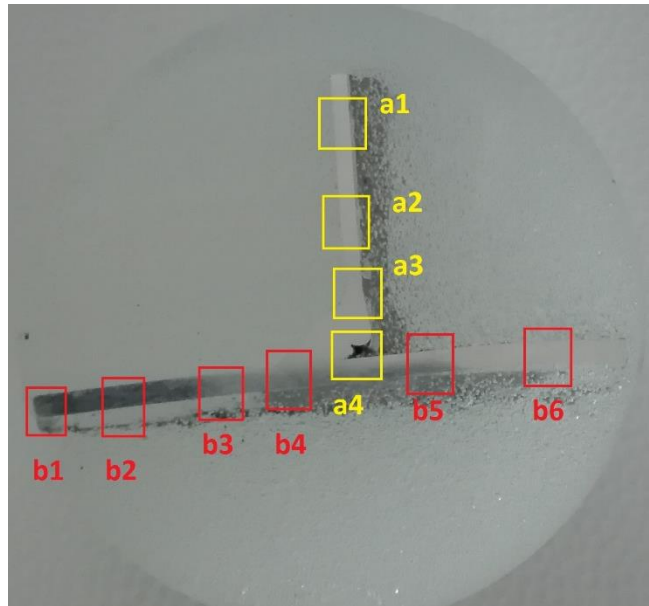Figure 31: Micrograph of HAZ areas in b-direction under 50x magnification a) b3 area consist of base metal and Heat affected zone b) b_4 area consist of Heat affected zone and welded metal.

(a)   (b)
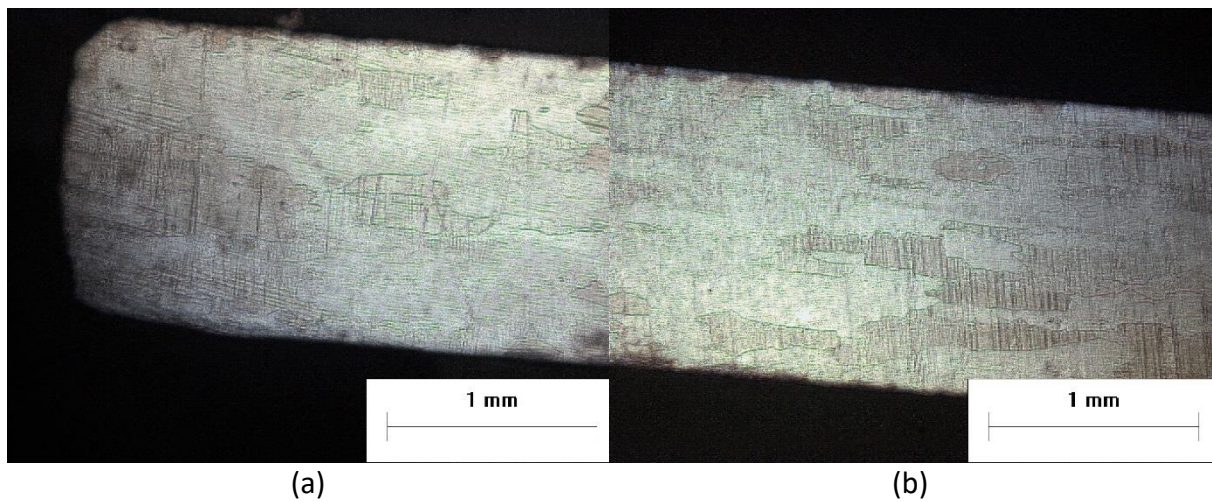
Figure 32: Micrograph of base metal areas in **b**-direction under 50x magnification a) b_5 area b) b_6 area.

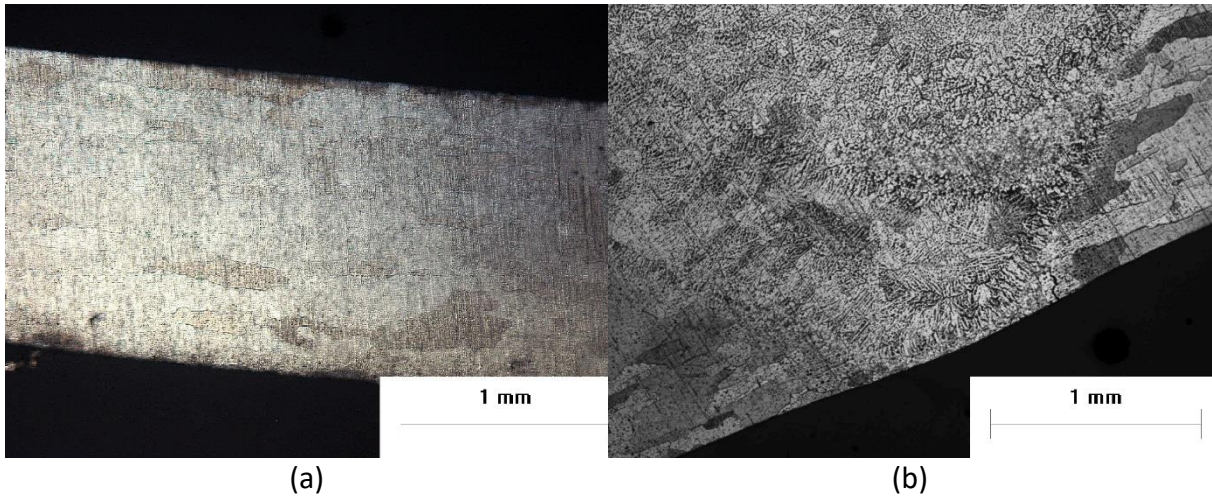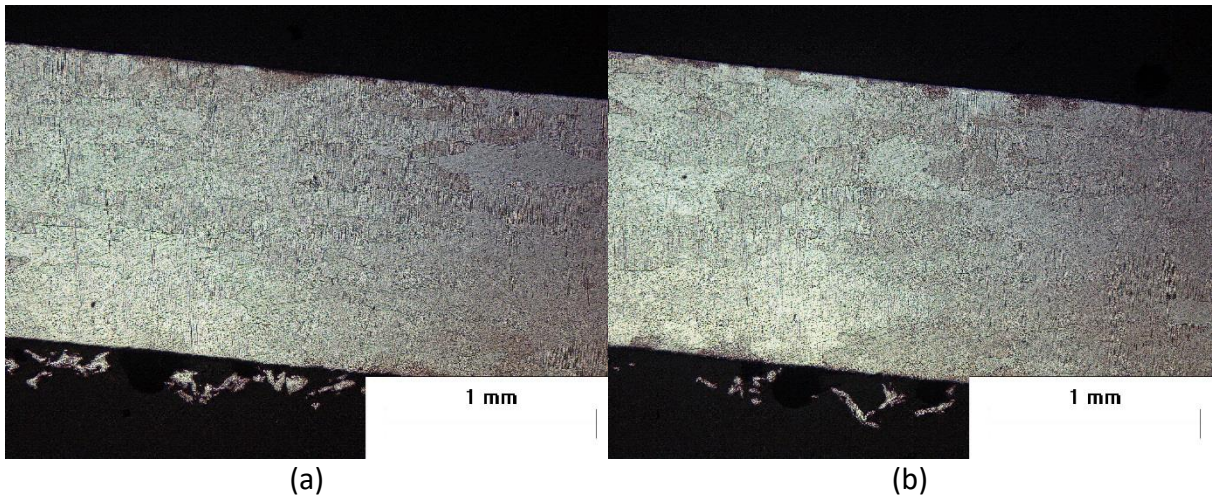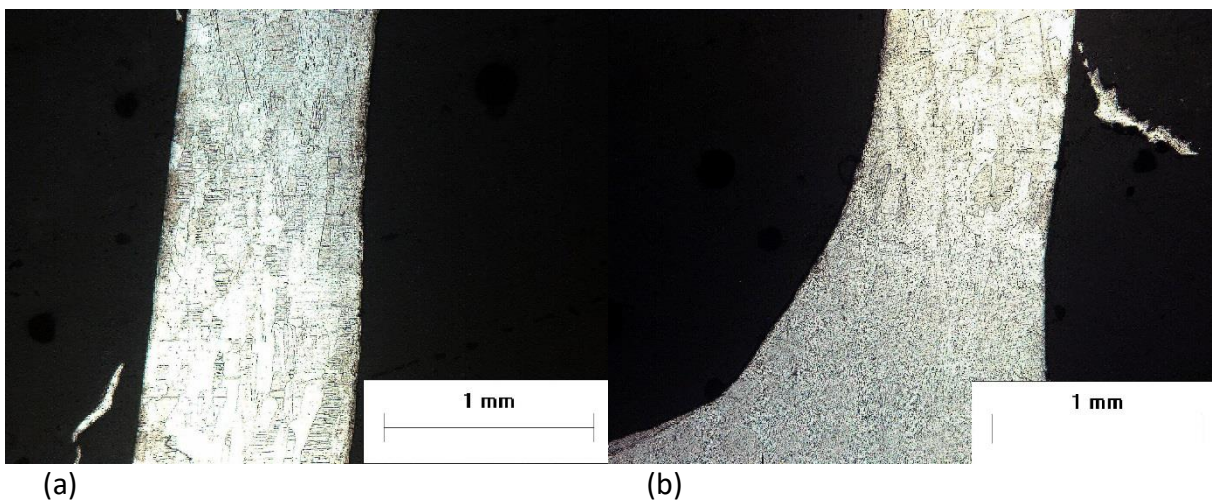(a)   (b)

Figure 33: Micrograph of base metal areas in **a**-direction under 50x magnification a) A_1 area consist of base metal b) A_2 area consist of base metal and Heat affected zone.
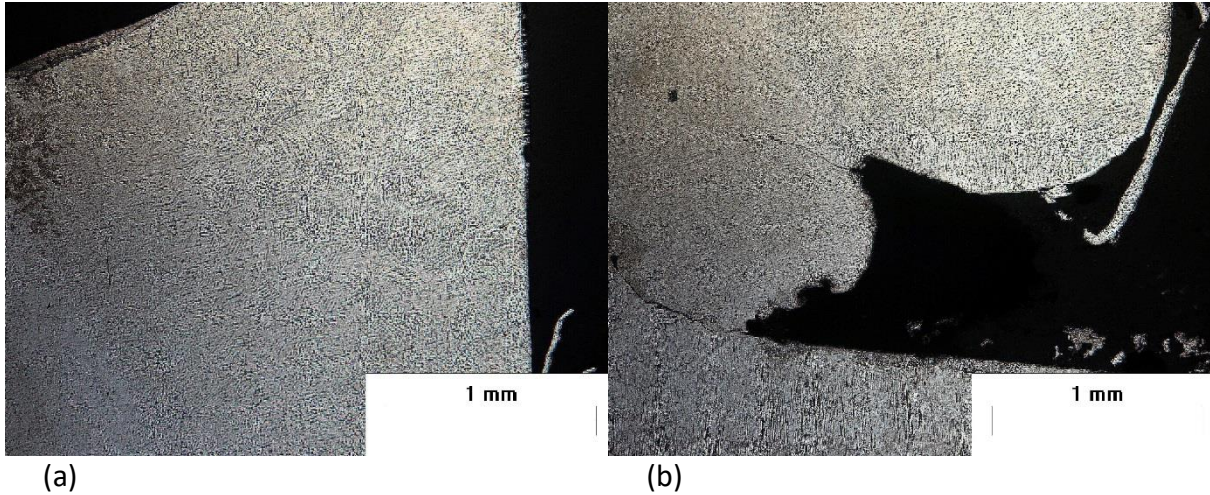
(a)   (b)

Figure 34: Micrograph of HAZ areas in **a**-direction under 50x magnification a) A_3 area consist of heat affected zone and welded metal b) A_4 area consist of heat affected zone and welded metal.

In the previous figures, there is an observation of the welding zones, where the big grains of the base metal are followed by more homogenized Haz grains, following the casting structure of the welding metal.

In further magnification and etching, we can observe better the boundaries of the welding zones, especially the ones between HAZ and welding metal (Figure 35 (b)). There the big grains of the HAZ are "interrupted" by the casting structure of the welding metal. As stated earlier the Haz-base metal boundaries are defined by the microhardness tests.

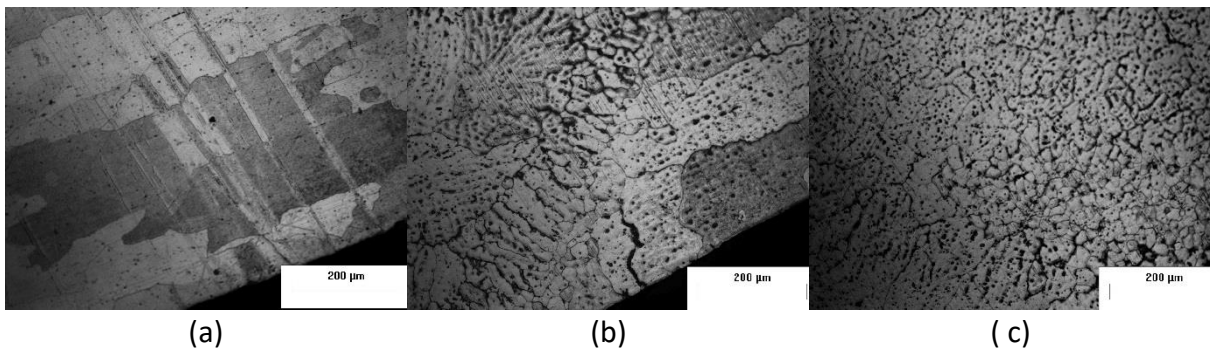(a)   (b)   (c)

Figure 35: Micrographs of welding zones under 200x magnification at a) Base metal, b) HAZ, c) welding point

The Table 10 displays the average grain size of each weld zone.

Table 10 Average grain size (μm) of T1-T1 7005 welding

Area	Average grain size (μm)
Base metal	100-200
HAZ	150-200
Welding point	Casting structure

41

4.3.3   Welding of 7005- T6 to 7005- T6 alloy (MIG).

Pipe 7005-T6 was welded to 7005-T6 keeping the same geometry as in the case of welding 7005-T1 to 7005-T1, described above in section 4.3.2. The same welding method was used (MIG welding). Figure 36 shows the areas, that were studied metallographically in the case of T6-T6 welding.
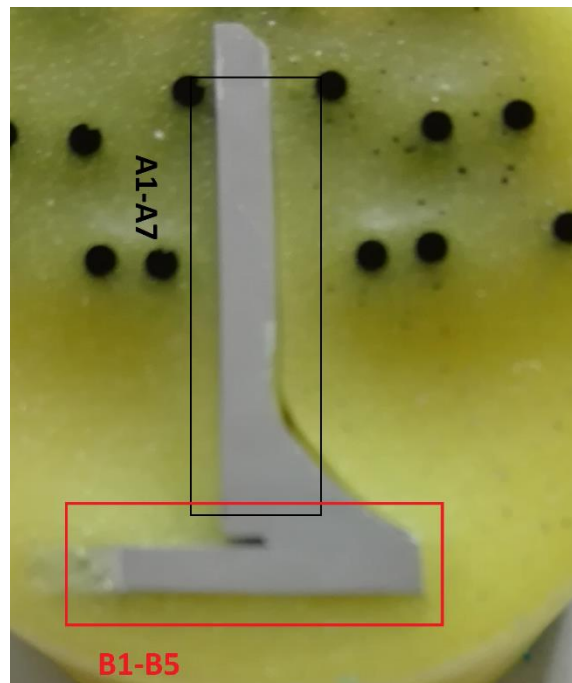

Figure 36: Studied areas of the MIG welding between the two 7005-T6 pipes.

The studied areas are presented in the figures below under 50x magnification.

| (a) | (b) | (c) |

Figure 37: Micrographs of 7005-T6 weld in **b**-direction. All micrographs are 50x magnification. a) Base metal, b_1 area. b) Base metal, b_2 area. c) Base metal, b_3 area.

Figure 38: Micrograph of 7005-T6 weld in **b**-direction. HAZ, b_4 area. Magnification is 50x.

Figure 39: Micrograph of welded metal in **b**-direction (b_5 area). Magnification is 50x.

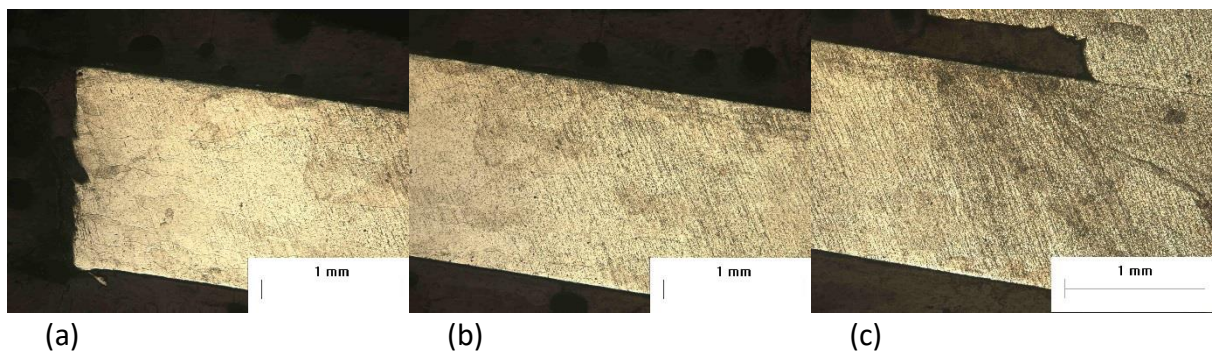
(a)   (b)   (c)
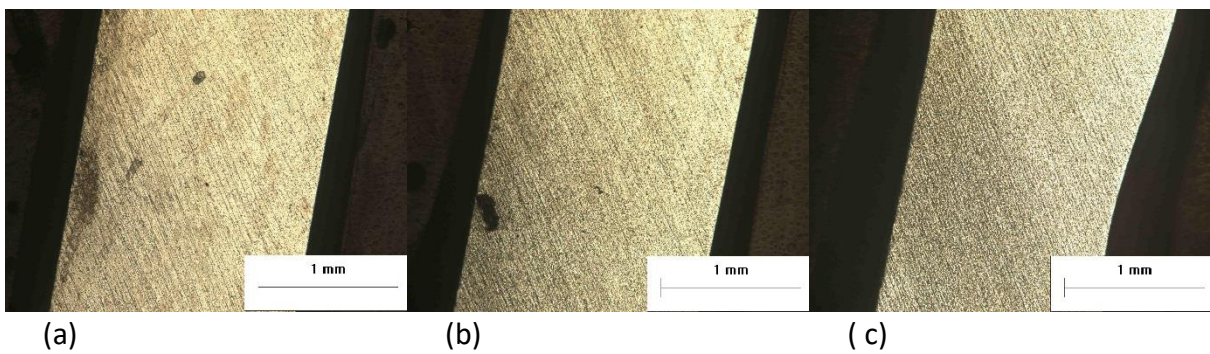
Figure 40: Micrographs of 7005-T6 weld in **a**-direction. All micrographs are 50x magnification.
a) Base metal of $a_1$area b) Base metal of a_2 area c) Base metal of a_3 area
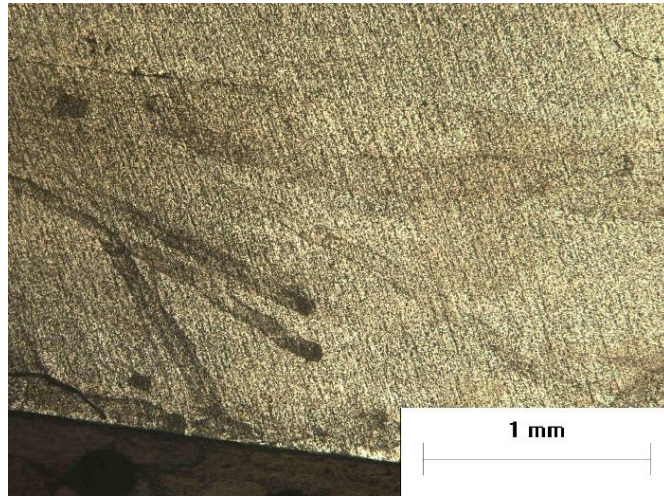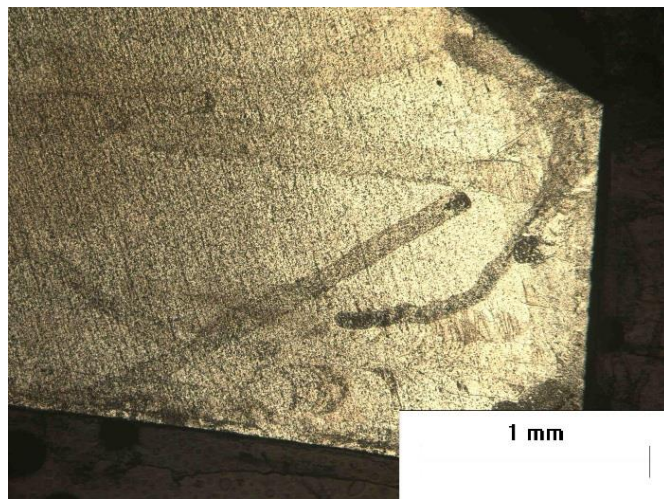
(a)   (b)
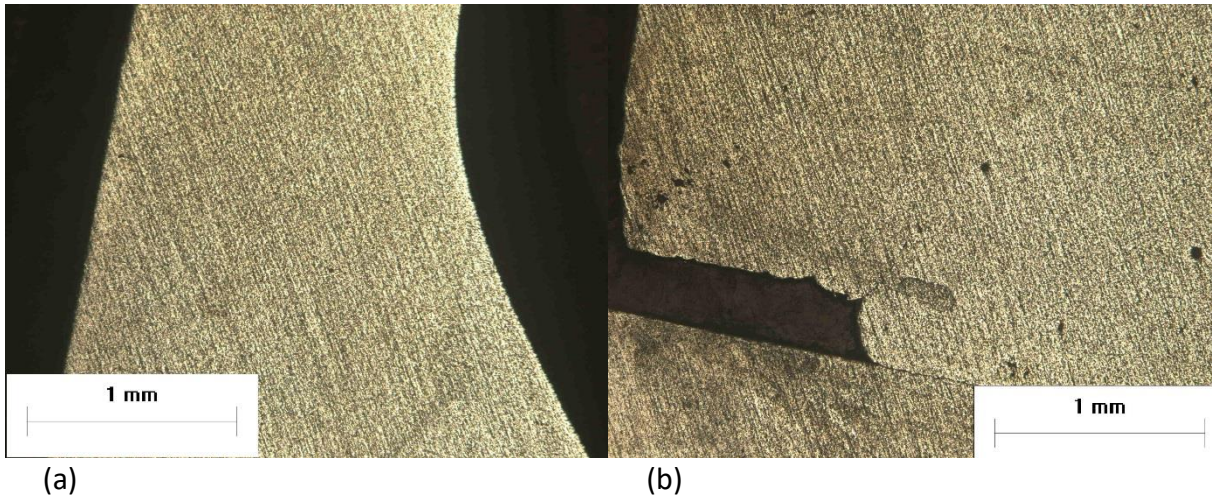
Figure 41: Micrograph of heat affected zone of **a**-direction under 50x magnification. a) A_4 area b) A_5.

(a)   (b)
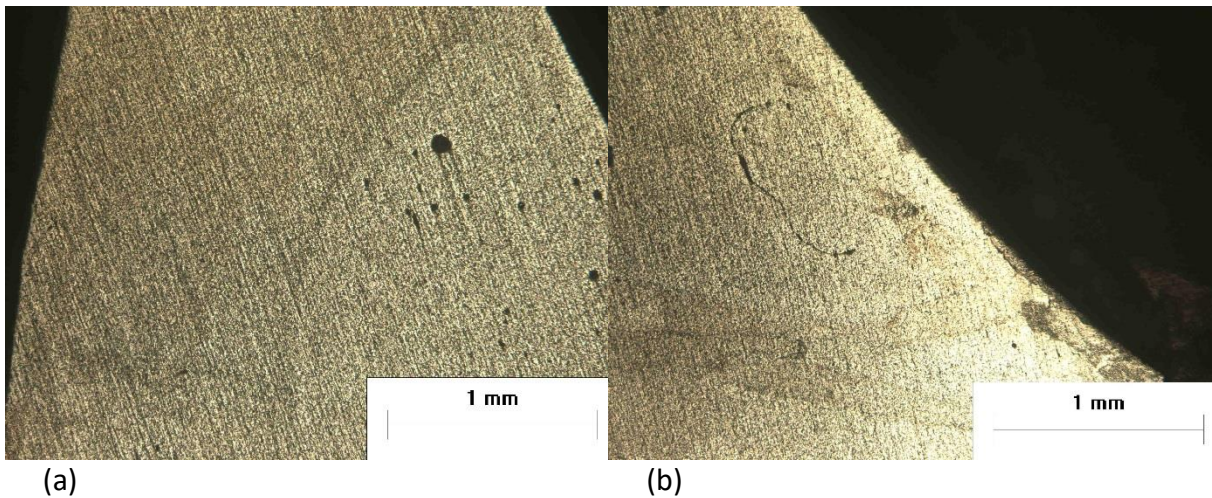
Figure 42:Micrograph of welded metal of **a**-direction under 50 x magnification a) A_6 area b) A_7 area.

As in the 7005-T1 weld, the base metal of the 7005-T6 consist of big grains with significant deviation, which are followed by the heat affected zone. The boundaries between those two zones aren't clear in the metallographic analysis. On the other hand, the boundaries between heat affected zone and the welding point are clear in Figure 42 (a) .

Table 11: Average grain size (µm) of T6-T6 7005 alloy

Area	Average grain size (µm)
Base metal	50-200
HAZ	100-200
Welding point	Casting structure

44

In order to study extensively the heat affected zone there was a second welding of the 7005-T6 pipe The welding was performed as it is shown in the Figure 43 and the metallography is presented in the following figures.

Figure 43: Macrograph of MIG welding 7005 T6 pipe.

(a)   (b)

Figure 44: Micrographs of base metal areas a) Magnification 50x b) Magnification 200x.

(a)   (b)   (c)

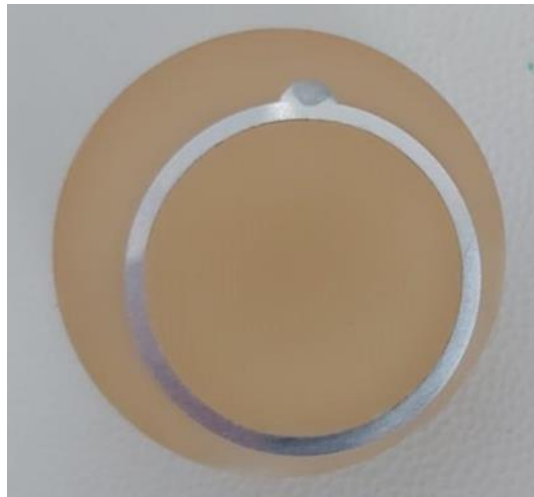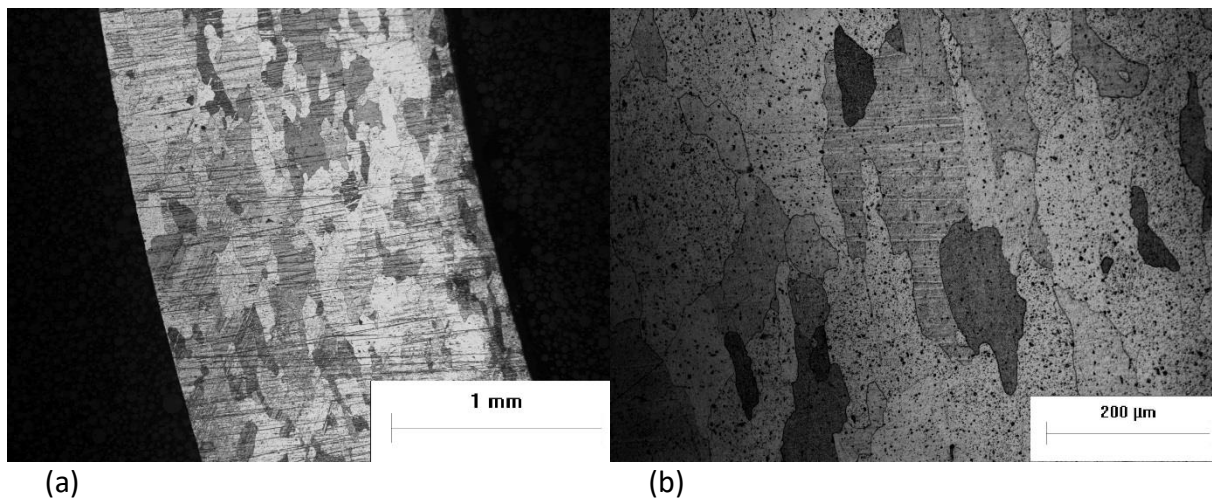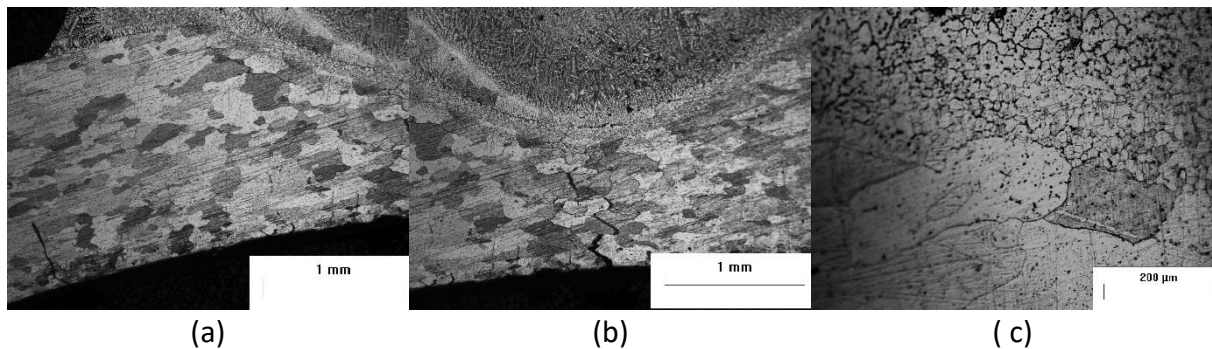Figure 45 : Micrographs of heat affected zone a) Magnification 50x b) Magnification 50x c) Magnification 200x.

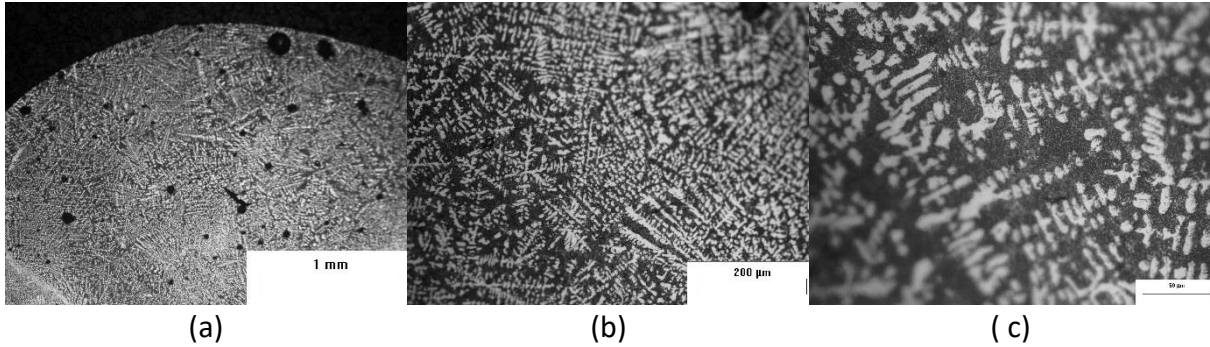|		
(a)	(b)	(c)

Figure 46: Micrographs of welded metal a) Magnification 50x b) Magnification 200x c) Magnification 500x

In the Figure 45(a) we can see the microstructure of the HAZ. The heat input has caused cracking in bottom side of the metal (Figure 45 (b)) were the welding has almost melted the metal. In the Figure 45(c) the grains of the HAZ have developed small columnal microstructures in their boundaries marking the beginning of the melted metal.

Figure 46 shows the welding point, were pores have developed inside the formed metal. This is caused by gas that has been trapped inside the liquid metal during its melting. The welding microstructure consist of casting columnal forms called dendrites which are formed due to the unevenly distributed cooling of the metal.

4.3.4 Welding of 7020 alloy (MIG).

The plate form 7020-T6-alloy weld was performed also by MIG process and the samples were cut vertically to the welding direction as shown at the Figure 47. The samples that were extracted are presented in the Figure 48, as well as the studied areas.
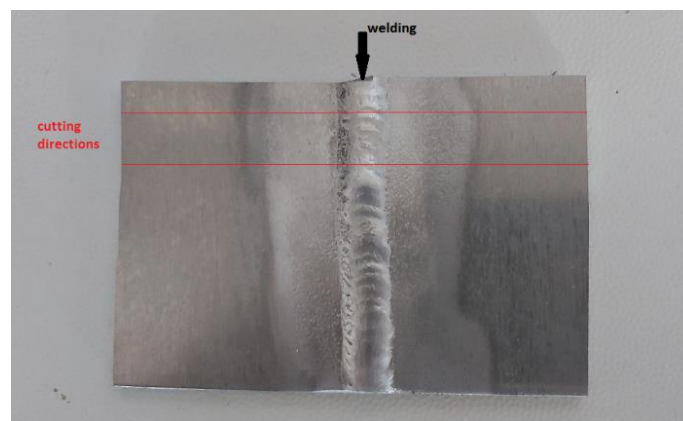
Figure 47: Cutting directions of the 7020 MIG welding. The red lines indicate the cutting direction, vertical to the weld.

46
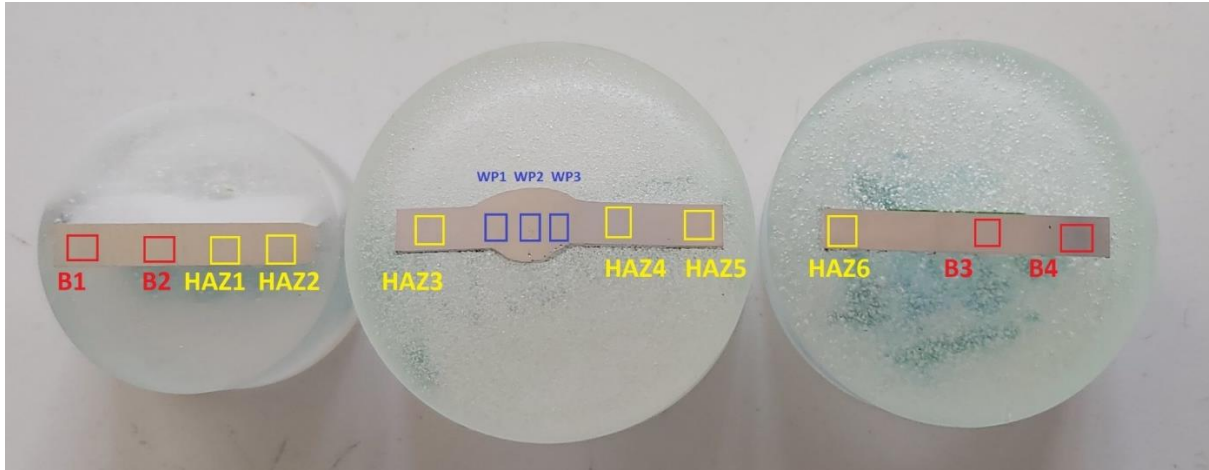
Figure 48: Areas that were studied for metallography. B1-B4 indicate the Base metal, HAZ1-HAZ6 present the heat affected zones and WP1-WP3 the welded metal.

The metallography of the studied areas is as presented below.

(a)   (b)

Figure 49: Micrographs of the areas representing the base metal in the left of the welding under 200x magnification a) B_1 area b) B_2 area.

(a)   (b)   (c)

Figure 50: Micrographs of the areas representing the heat affected zone in the left of the welding under 200x magnification a) HAZ_1 b) HAZ_2 c) HAZ_3

47

(a)   (b)   (c)
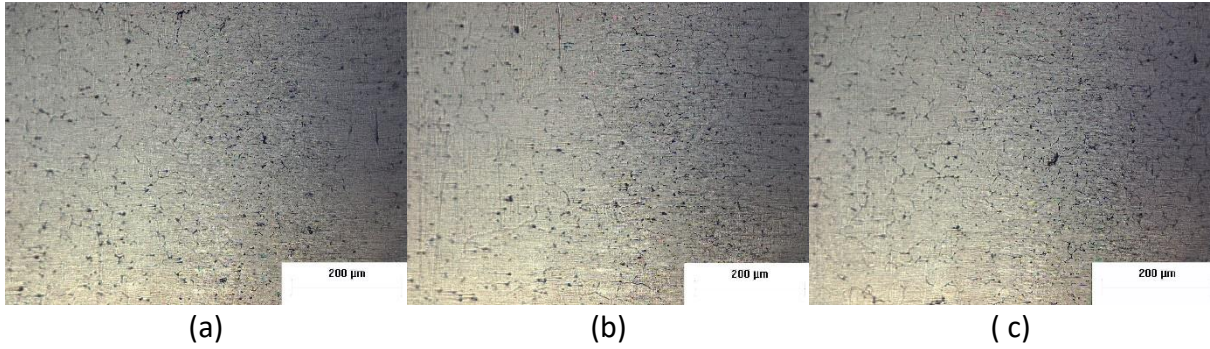
Figure 51 : Micrographs of the areas representing the welded metal under 200x magnification a) WP_1 b) WP_2 c) WP_3

(a)   (b)   (c)
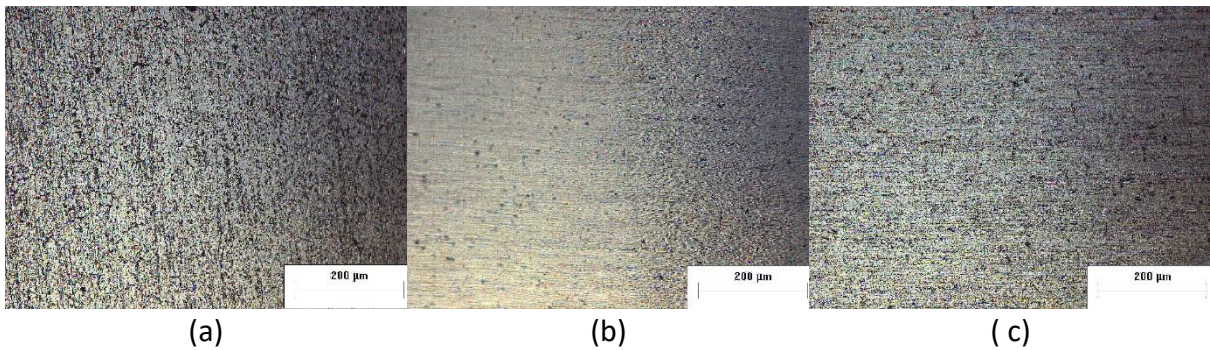
Figure 52 : Micrographs of the areas representing the heat affected zone in the right of the welding under 200x magnification a) HAZ_4 b) HAZ_5 c) HAZ_6

(a)   (b)

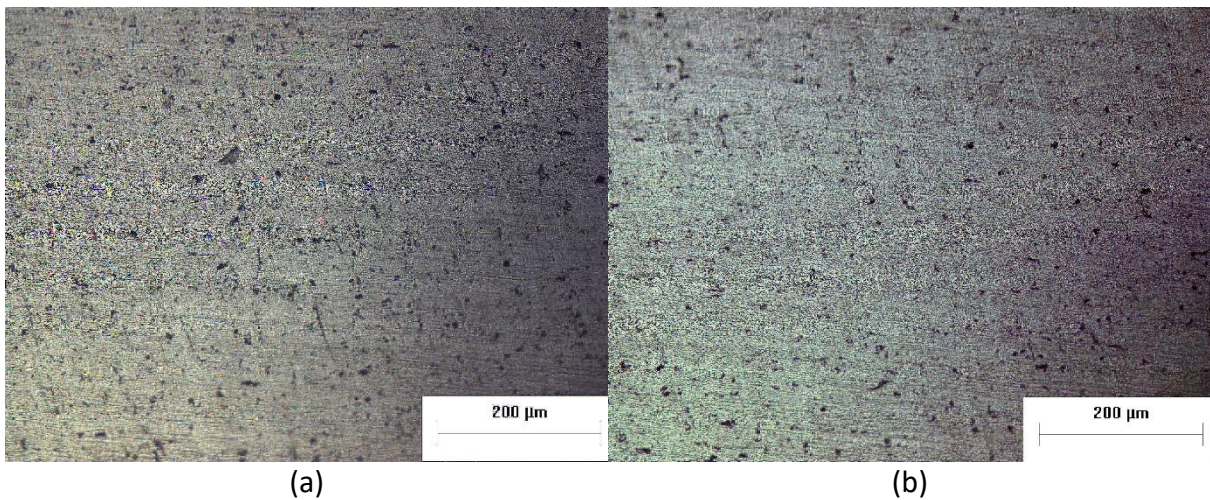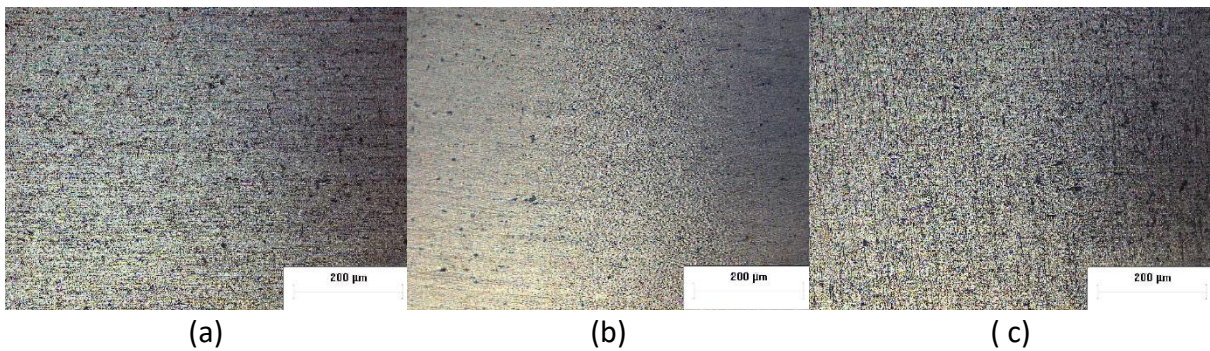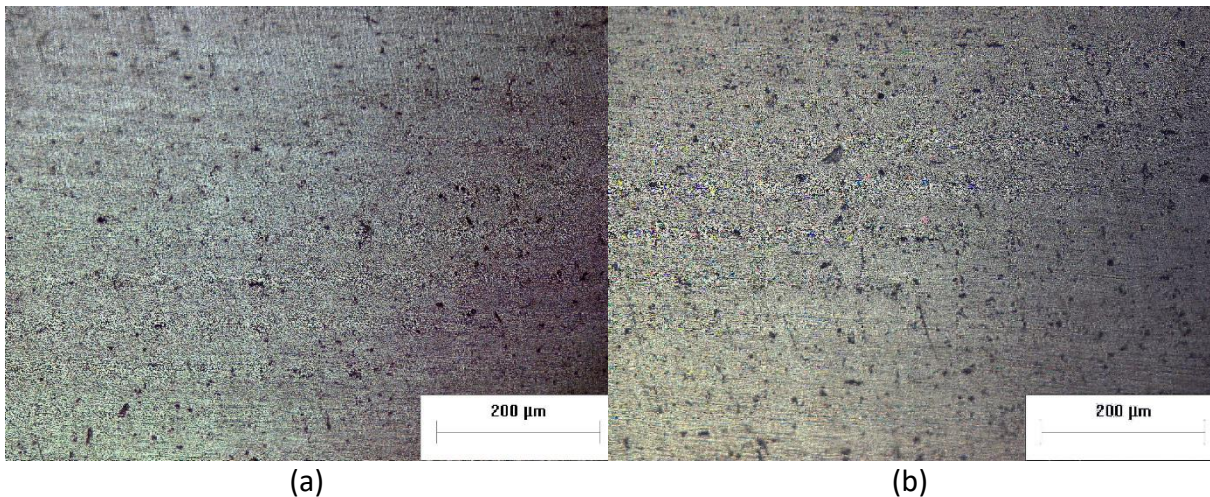Figure 53: Micrographs of the areas representing the base *metal in the left of the* welding under 200x magnification a) B_3 area b) B_4 area

The 7020-T6 weld doesn't present any significant differences in metallography with the 7005. Again the base metal is unaffected by the heat input of the welding process , the heat affected zone can't be seen in the optical microscope and the boundaries between the welding point and the heat affected zone are shown in Figure 51.

The average grain size of the welding areas is presented in Table 12.

48

Table 12 Average grain size (μm) of 7020-T6 alloy weld

Area	Average grain size (μm)
Base metal	80-120
HAZ	100-150
Welding point	Casting structure

4.3.5 Post Weld Heat Treatment Simulation of 7005-T1 base metal

As stated earlier the microstructure of the 7005-T1 alloy after 2, 6, 10, 24 and 42 hours at 120°C, is presented in Figure 54-Figure 58 under 50x and 200x scale.

(a)   (b)

Figure 54: Microstructure of 7005-T1 alloy after 2 hours at 120°C a) Magnification 50x b) Magnification 200x

(a)   (b)

Figure 55: Microstructure of 7005-T1 alloy after 6 hours at 120°C a) Magnification 50x b) Magnification 200x.

(a)   (b)

Figure 56: Microstructure of 7005-T1 alloy after 10 hours at 120°C a) Magnification 50x b) Magnification 200x
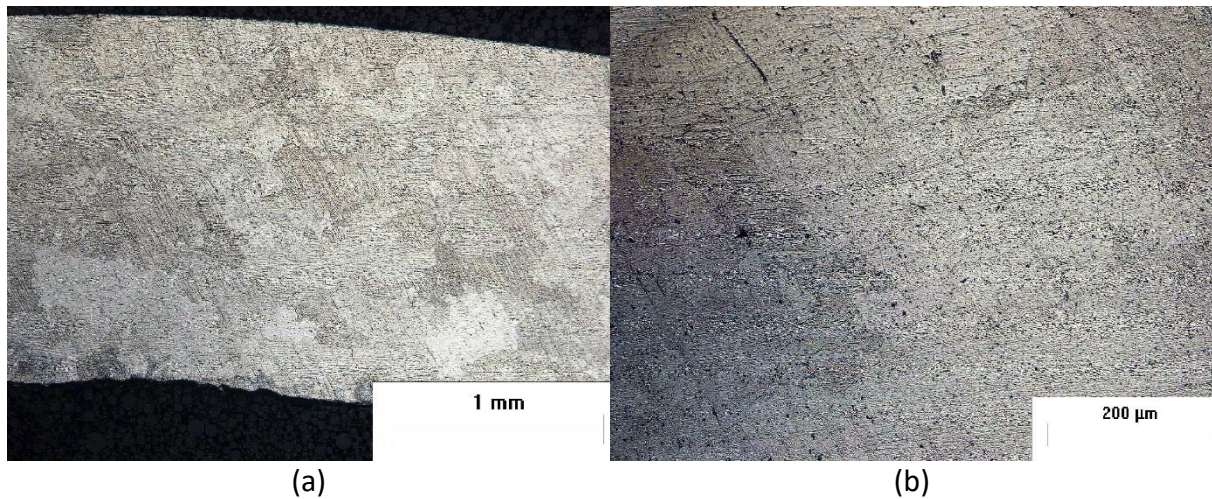

(a)   (b)

Figure 57: Microstructure of 7005-T1 alloy after 24 hours at 120°C a) Magnification 50x b) Magnification 200x

(a)   (b)

Figure 58: Microstructure of 7005-T1 alloy after 42 hours at 120°C a) Magnification 50x b) Magnification 200x

As it is observed in the previous figures the microstructure of the metal in each time removal isn't changing significantly from the original material's. However, we can see a homogenization in the highest and lowest value of the metal's grain size. Therefore, the post weld heat treatment of the base metal doesn't change its microstructure. These conclusions are presented in the following table.

Table 13: Average grain size (μm) for T1 7005 samples.

Sample	Average grain size (μm)
As received (longitudinal)	200-550
As received (transverse)	50-150
After 2 hours (120°C)	60-150
After 6 hours (120°C)	70-160
After 10 hours (120°C)	130-170
After 24 hours (120°C)	100-150
After 42 hours (120°C)	90-150

4.3.6 Post Weld Heat Treatment Simulation of 7005-T6 base metal

The figures of the as received specimens follow the heat treated ones (2, 6, 10, 24 and 42 hours at 120°C) in the figures bellow (Figure 59-Figure 63) in 50x and 200x magnification.

(a)   (b)

Figure 59: Microstructure of 7005-T6 alloy after 2 hours at 120°C a) Magnification 50x b) Magnification 200x
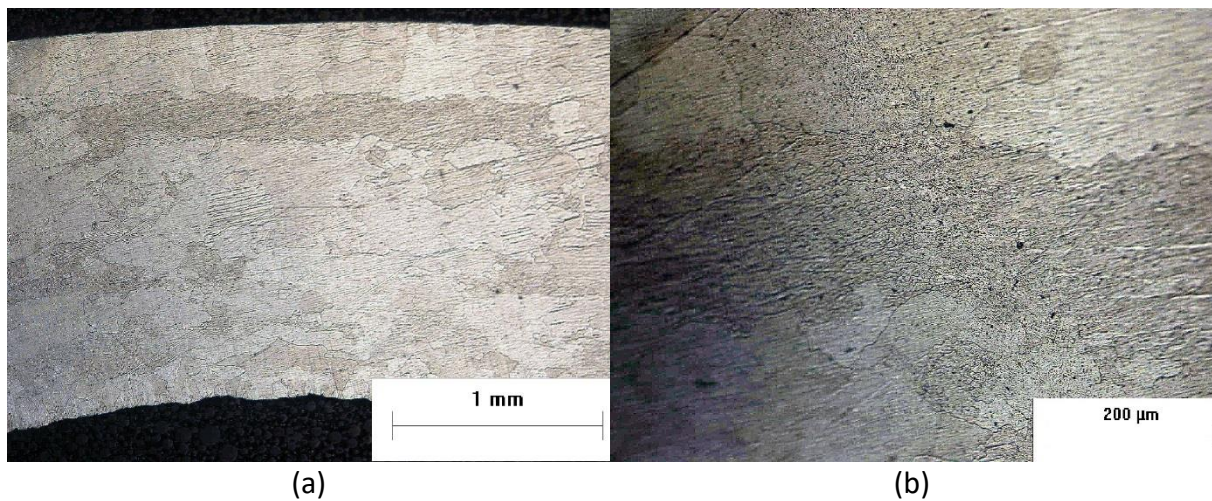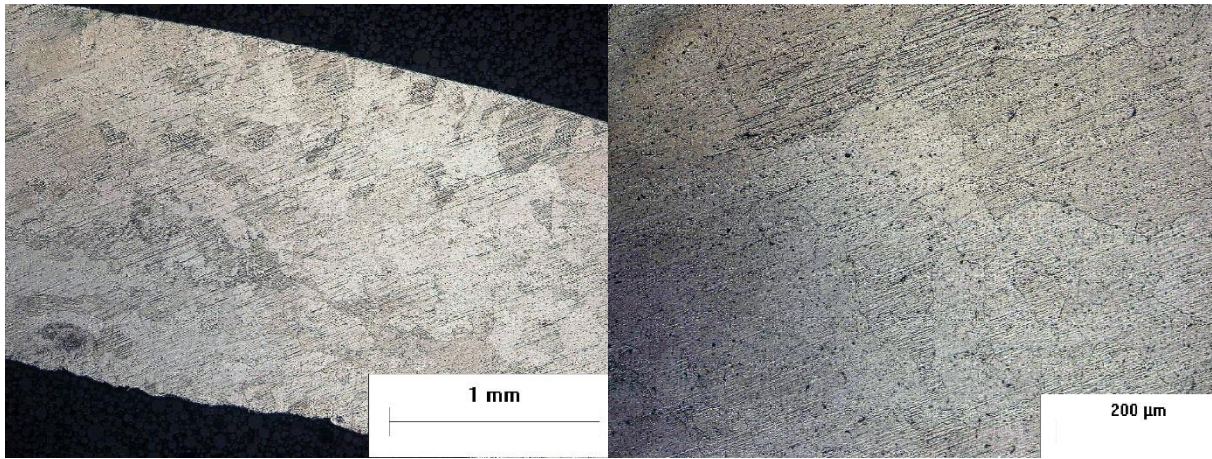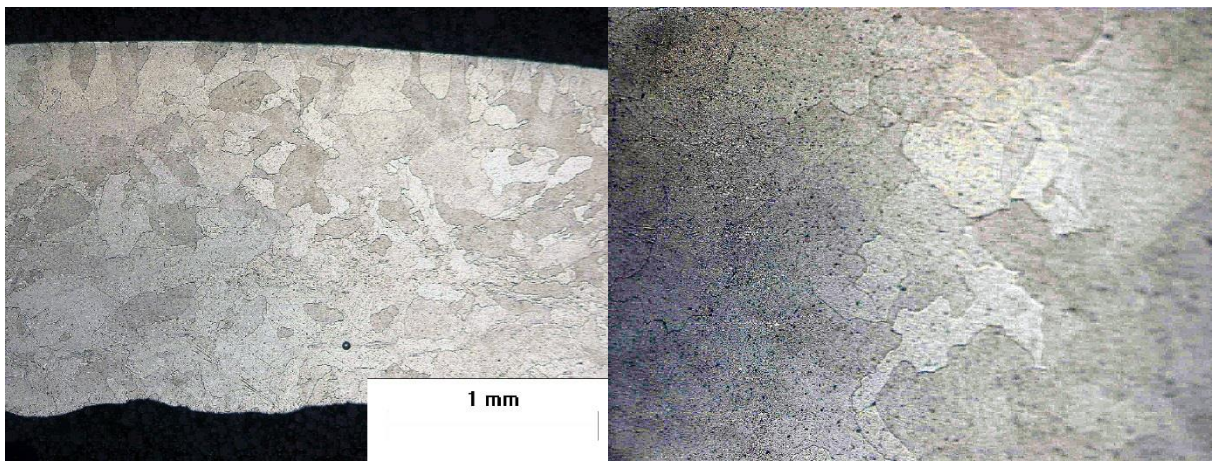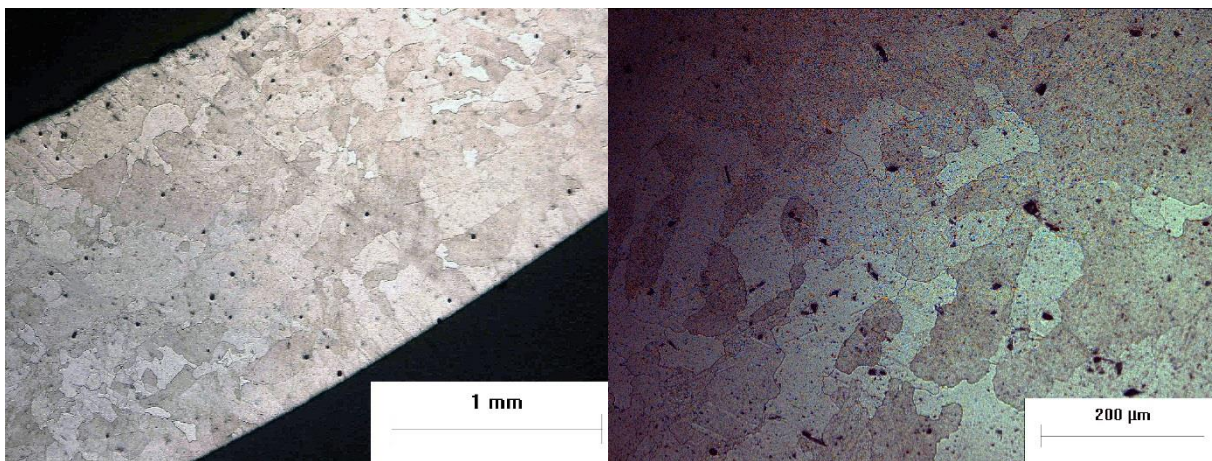
(a)	(b)

Figure 60: Microstructure of 7005-T6 alloy after 6 hours at 120°C a) Magnification 50x b) Magnification 200x.

(a)	(b)
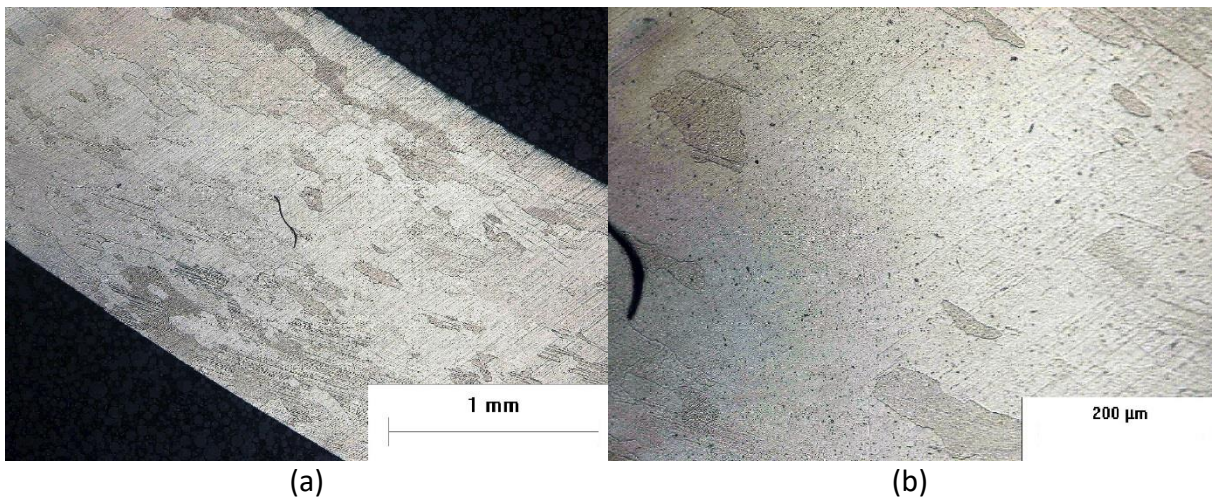
Figure 61: Microstructure of 7005-T6 alloy after 10 hours at 120°C a) Magnification 50x b) Magnification 200x

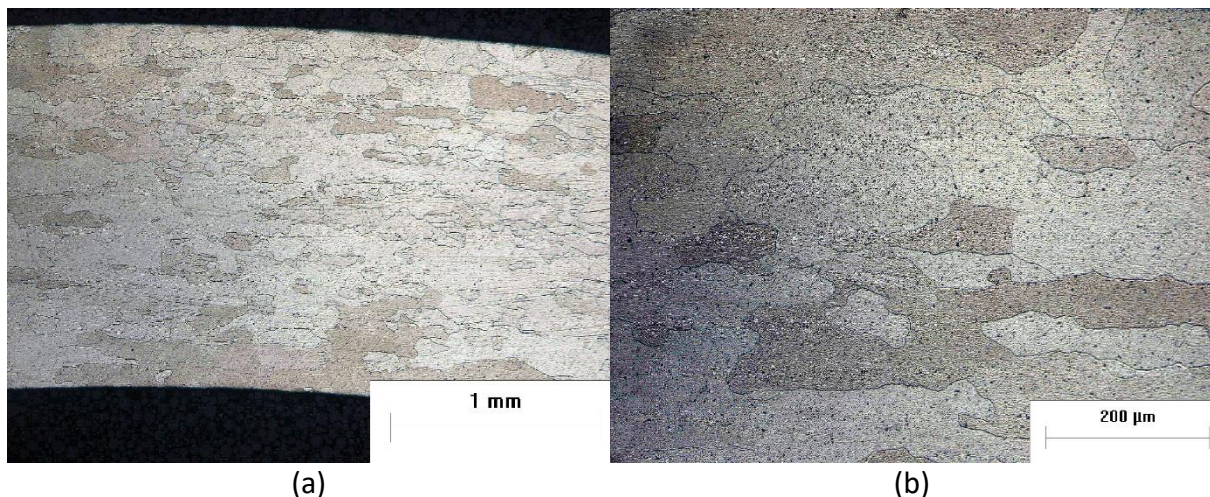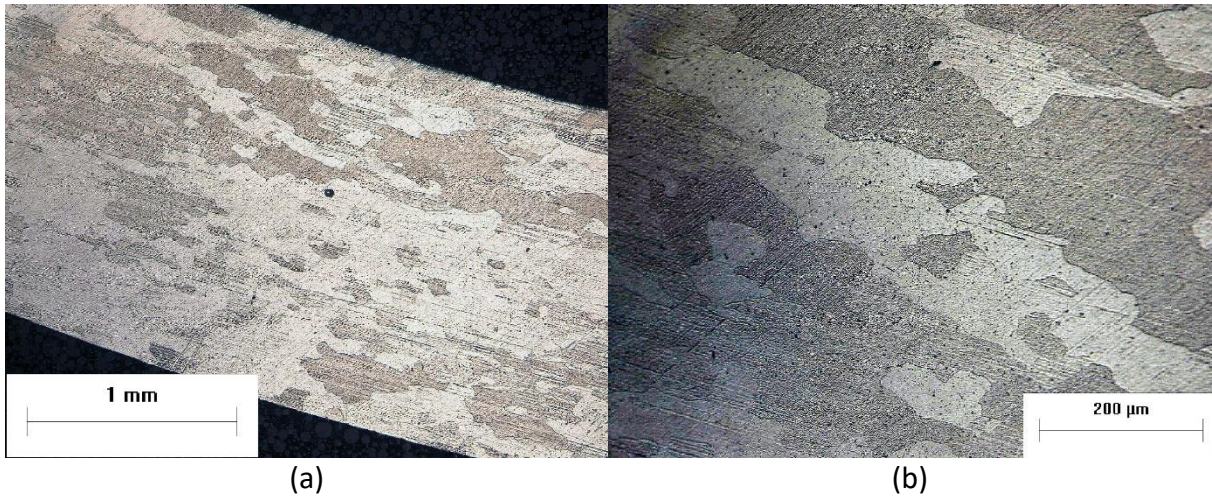
(a)	(b)
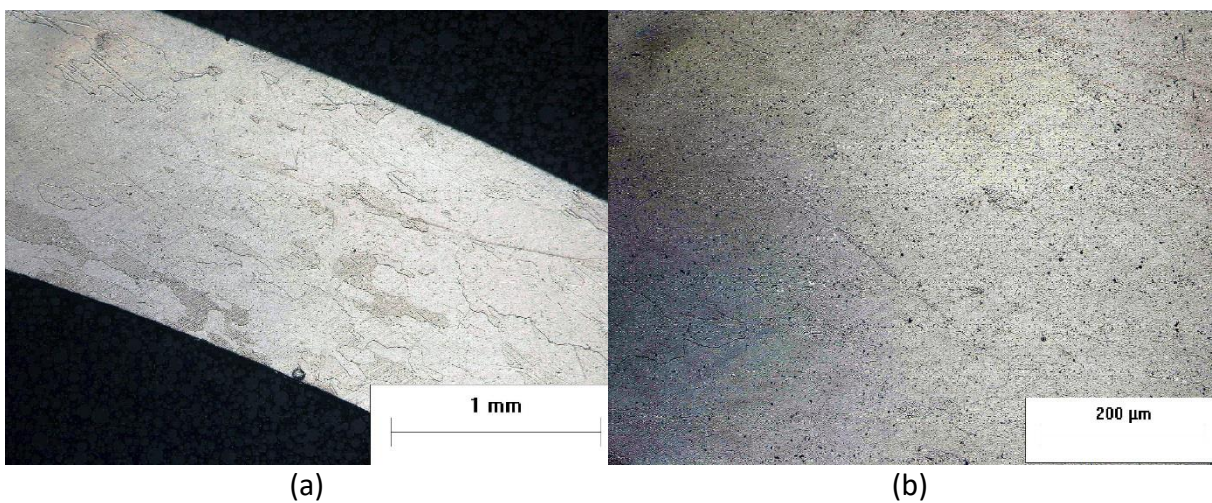
Figure 62: Microstructure of 7005-T6 alloy after 24 hours at 120°C a) Magnification 50x b) Magnification 200x

53

| (a) | (b) |
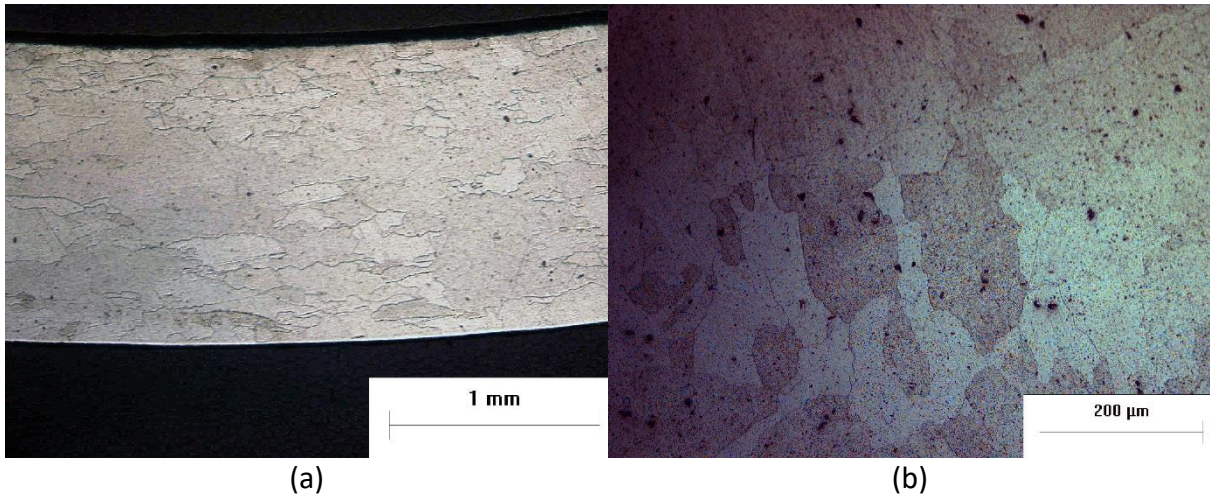
Figure 63: Microstructure of 7005-T6 alloy after 42 hours at 120°C a) Magnification 50x b) Magnification 200x

In 7005-T6 samples there is also an homogenization in the highest and lowest value of the grain size according to the time removal, but the average grain sizes remains the same (Table 14). As a result, we can assume that the post weld heat treatment of the 7005-T6 base metal doesn't affect its microstructure.

Table 14: Average grain size (μm) for T6 7005 samples.

Sample	Average grain size (μm)
As received (longitudinal)	150-400
As received (transverse)	30-170
After 2 hours (120°C)	50-180
After 6 hours (120°C)	70-170
After 10 hours (120°C)	70-150
After 24 hours (120°C)	100-150
After 42 hours (120°C)	110-170

54

4.4   Microhardness Measurements

The microhardness of the of the metal depends on the size and spreading of the precipitates that have been developed during the heat treatment of the material. Depending the peak temperature that the material has suffered, the precipitates can take the following forms. (Figure 64).

Figure 64: TEM micrographs directly after heat treatments depending the peak temperature a) base metal b)200°C c)300°C d)400°C [29].

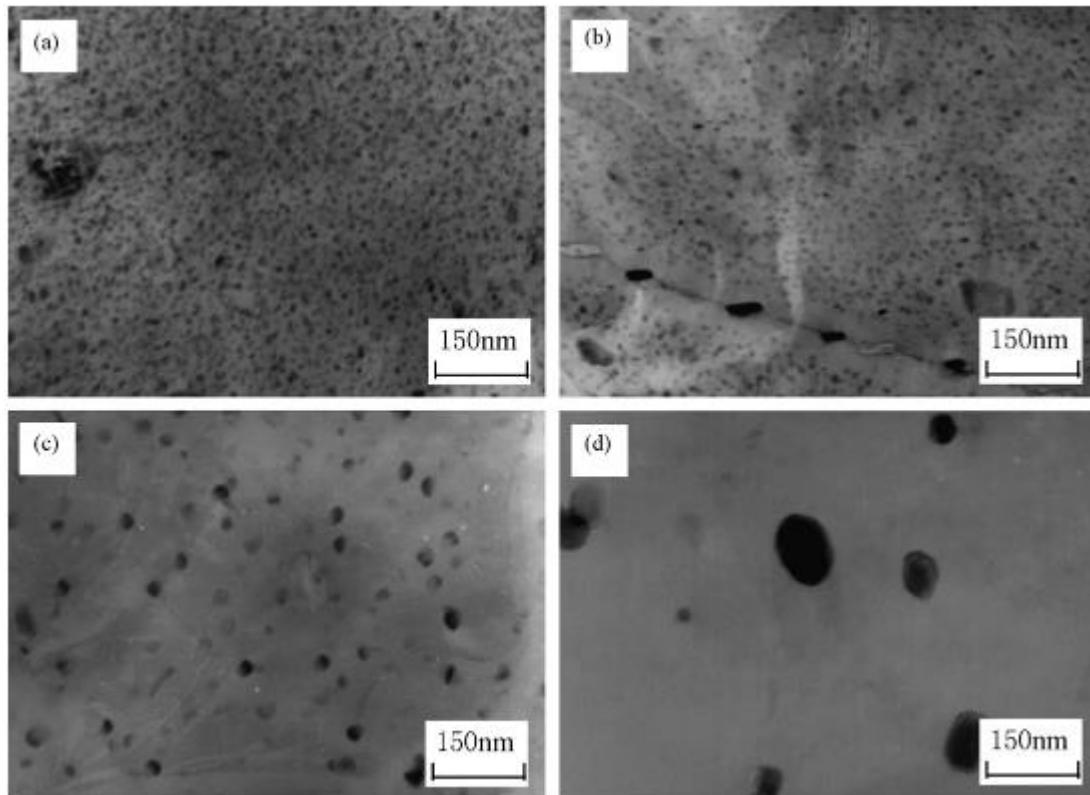As we can conclude from the figures above, the highest temperatures cause bigger and more isolated precipitates which decrease the microhardness as it will be presented in the following subsections.

4.4.1 Microhardness measurments of T1-T6 7005 welded alloy .

The 7005-T1-T6 welding has a semi-cylindrical cross section. As it is shown in the Figure 65 the direction of the hardness measurements is presented according to the distance from the welding point. At the left of the welding is the T1 alloy and at the right the T6. The microhardness test (Figure 66) shows the drop of the hardness values near the welding (HAZ) and the minimum values at the welding point. Far from the welding point the base metal is unaffected as expected. As we can observe the base metal has a hardness of 110-120 HV, the heat affected zone 80-100HV depending on the distance from the welding point and the welded metal has the lowest value of approximately 70 HV.
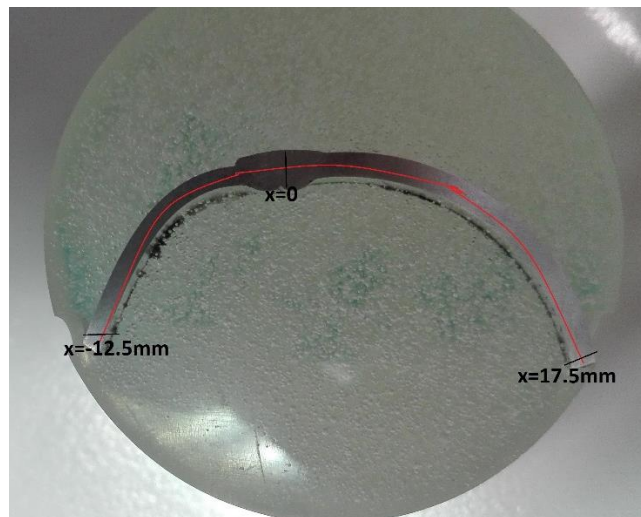

Figure 65: Macrograph of the MIG welding between 7005-T1 and 7005-T6 samples, showing the direction of microhardness measurements. The area left of the weld consist of 7005-T1 material and the area at the right consist of 7005-T6 material.
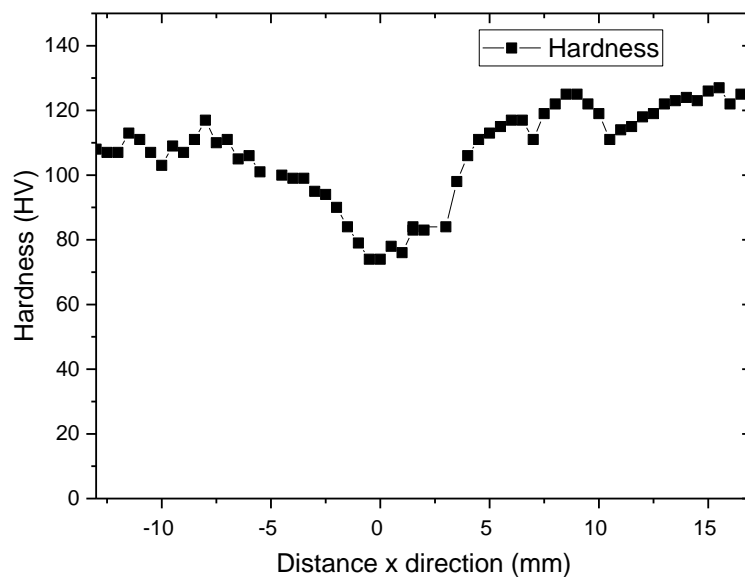

Figure 66: Microhardness measurements of 7005-T1-T6-alloy welding related to the distance from the weld (left 7005-T1 material, right 7005-T6 material)

4.4.2 Microhardness measurements for T6-7005 welded alloy.

As stated earlier, there were two 7005-T6 MIG welds.

In the first one the two pipes were joint vertically and the direction of the microhardness measurements is shown at the Figure 67. The results of the measurements are presented in Figure 68. As we can see, in the Figure 68 (a) in the y-direction the microhardness reduces at 1,5 mm indicating the heat affected zone, followed be the minimum values of the hardness in welding metal (2mm-5.5 mm). In Figure 70 (b) we can see that the values drop significantly fast, entering the heat affected zone and the welding metal.

As a result, we can say that the hardness of base metal ranges between 125 and 135 HV, the heat affected zone between 80 and 100HV and the welded metal between 60 and 70HV.
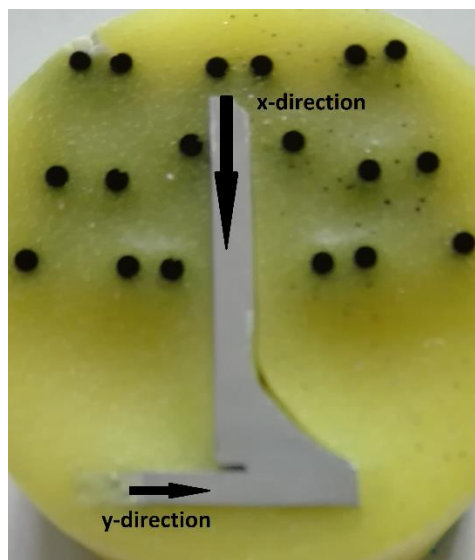

Figure 67: Direction x-y of T6 welding

(a)   (b)
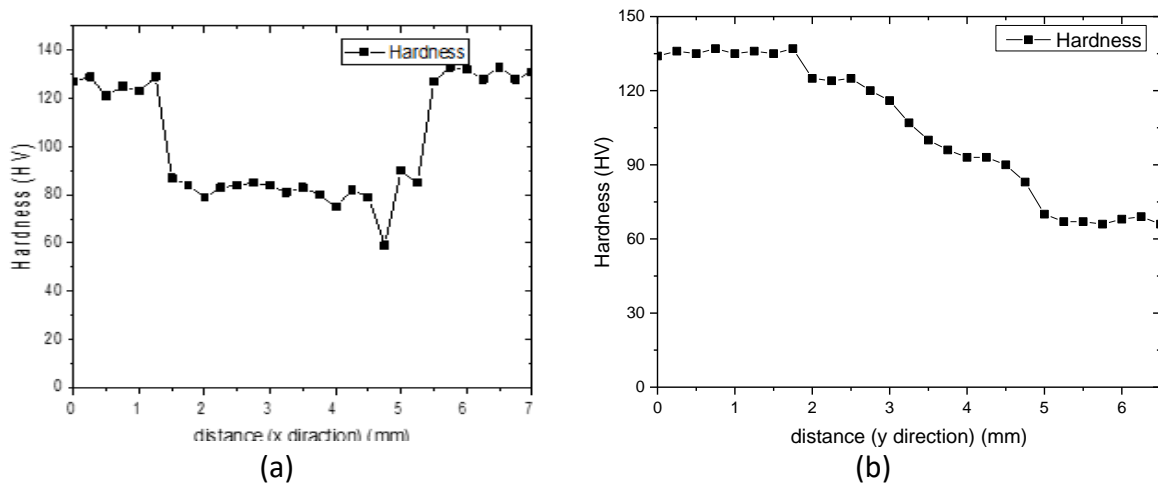
Figure 68: Microhardness measurements of the weld between the7005-T6 alloys welding: a) At x-direction, b) At y-direction.

The second 7005-T6 MIG welding consist of a pipe that has a joint on it's surface. This joint has affected a large area of the pipe as presented in Figure 70 in areas even 30mm far from the welding point.
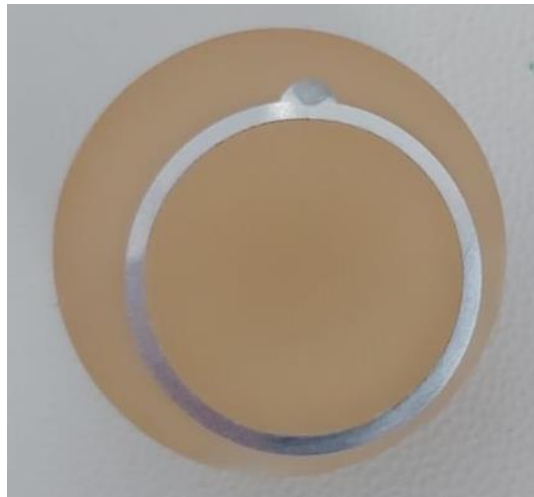
Figure 69: Macrograph of the second welding of the 7005-T6 pipe.
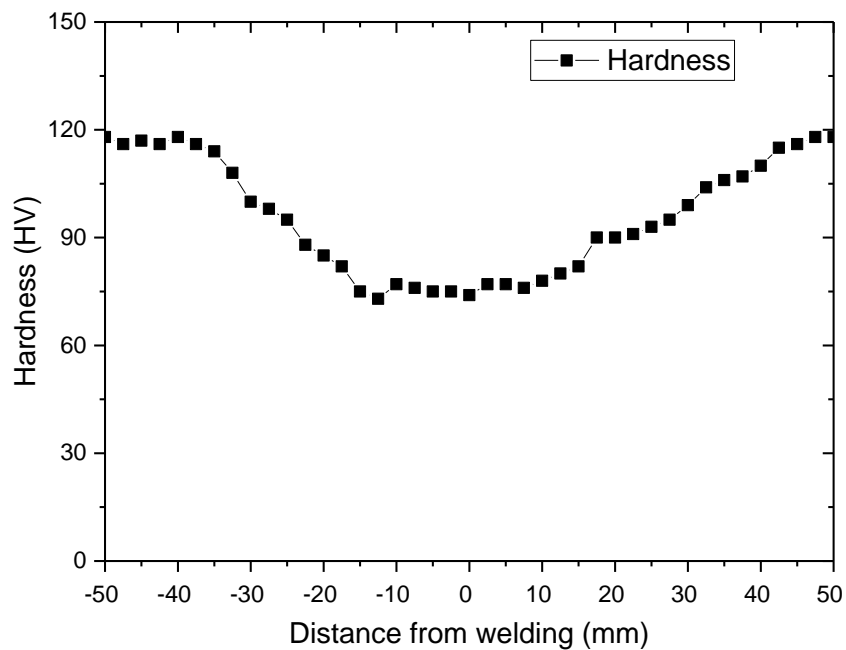
Figure 70: Hardness profile of MIG welding of 7005-T6 pipe according to the distance from the welding.

As we can see in the Figure 70 the hardness of the pipe has reduced in an area of 30mm far from the weld point, marking the heat affected zone. The microhardness range is 80-100 HV for the heat affected zone. The welded metal has lower hardness between 70 and 80 HV and the base metal hold is higher hardness of 120 HV.

After the artificially ageing at 120°C for 12,24 and 42 hours, we can observe that there is a rise in the microhardness of the heat affected zone and the welding metal. Therefore, there is a short area inside the heat affected zones that stays unaffected by the ageing process.

4.4.3 Microhardness measurements of T1-7005 welded alloy

The 7005-T1 welding was performed by joining the two pipes vertically and the directions of the hardness measurements are shown in Figure 71. The results are presented in the following figures.
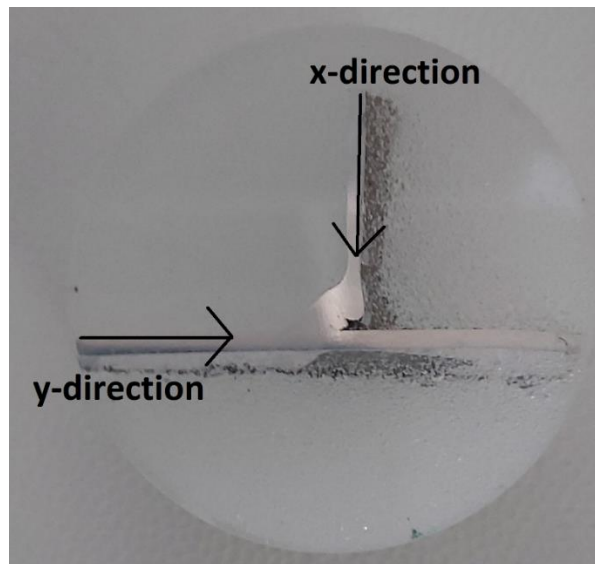
Figure 71: Macrograph of the welding between the 7005-T1 pipes showing the directions of microhardness measurements.

In Figure 72 we can see the hardness test of the weld in the two directions. As we can observe, the base metal of 7005-T1 material holds its hardness of 95-105HV. The heat affected zone of this weld includes a smaller area than in 7005-T6 with hardness values between 85 and 95 HV. In the welding point the microhardness drops to 80HV.


(a)　　　　　　　　　　　(b)

59
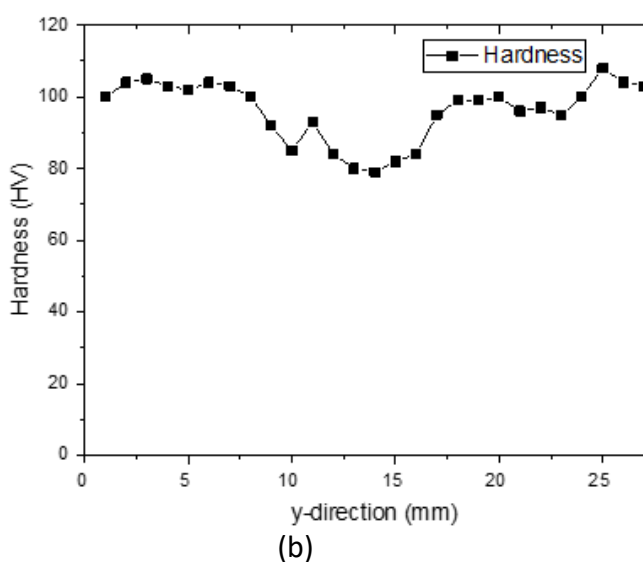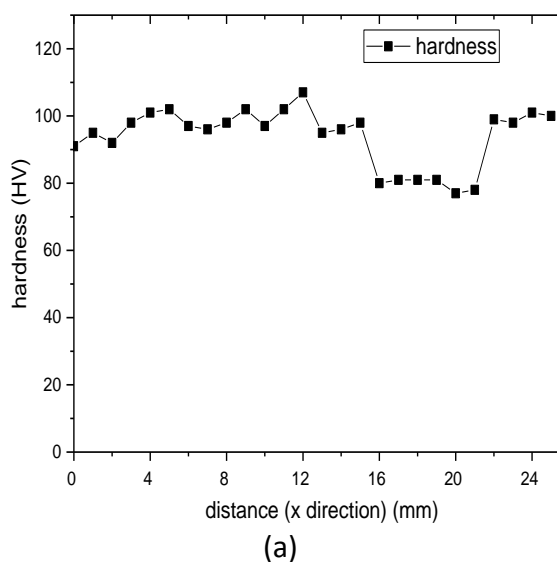
Figure 72: Microhardness profile of the weld between the 7005-T6 pipes at: a) x-direction, b) y-direction.

4.4.4   Microhardness measurements of 7020 welded alloy

In the 7020 welding (Figure 73**Error! Reference source not found.**) the microhardness measurements according to the distance from the welding are presented in the Figure 74. Again, the hardness at the heat affected zone (80-90HV) drops lower to the basic metal's (100-105HV), followed by further drop in the welding point (75HV). Therefore, the respond of the 7020 hardness profile is similar to the profile of the 7005.

Figure 73: Macrograph of the 7020 alloy welded sample.
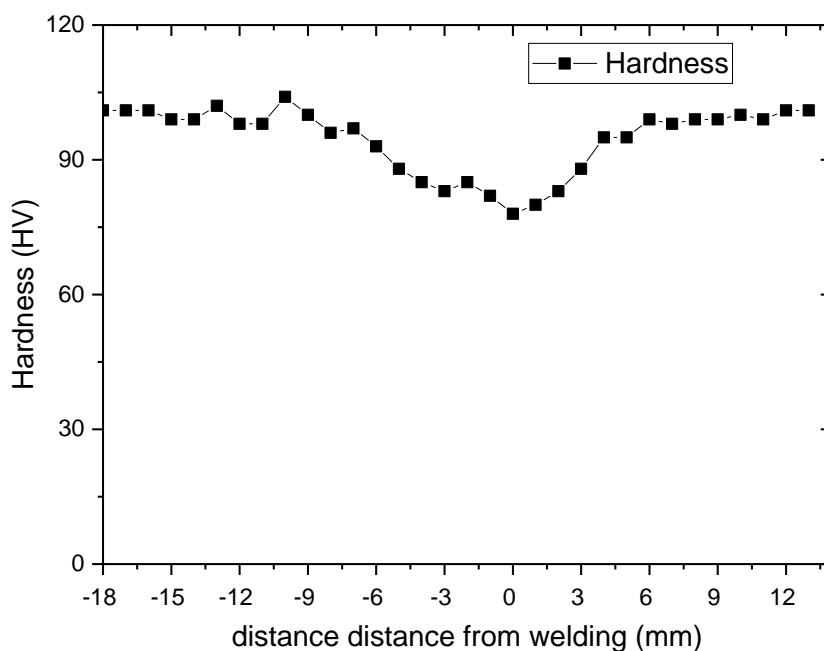
Figure 74:Microhardness profile of the 7020-alloy welding.

4.4.1 Microhardness measurements of Post Weld Heat Treatment Simulation of 7005-T1 and T6 base metal

As we can observe in Figure 65 the hardness of 7005-T1 alloy isn't affected by the heat treatment that it suffers. On the other hand, in Figure 66 the hardness of 7005-T6 reduces from 115 HV to 85 HV during the first 10 hours of the heat treatment and after that it retrieves its hardness again in 24 hours. Its final hardness rises to 130 HV in 42 hours.

Figure 75: Hardness profile of 7005-T1 simulated base metal specimens according ageing time (HV).

Figure 76: Hardness profile of 7005-T6 simulated base metal specimens according ageing time (HV)

4.4.2 Microhardness measurements of 7005 HAZ simulation and Post weld heat treatment.

As stated earlier different samples from the 7005 material as received were extracted in order to be simulated by appropriate heat treatment with the heat affected zone of the 7005-welding. The microhardness of each sample defines the area in the heat affected zone that it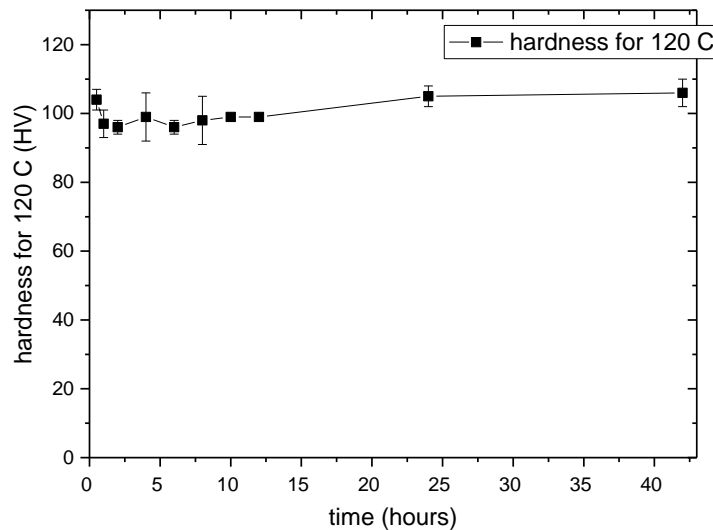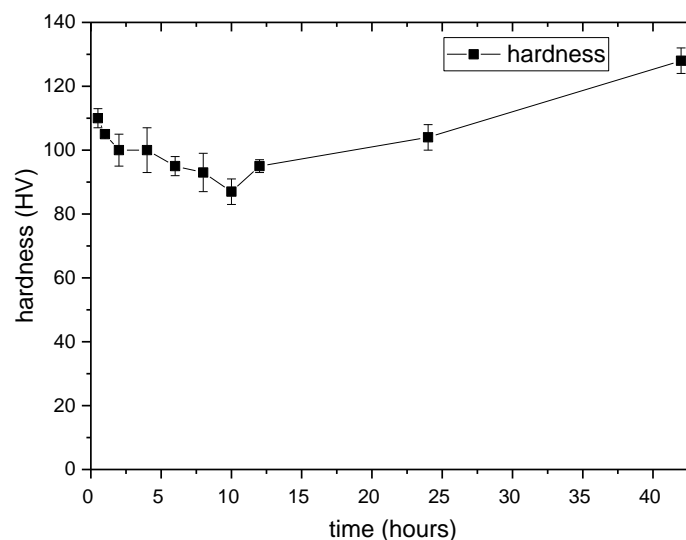 submits. In Figure 77 is presented the microhardness of each sample exposed from 150-550°C. As we can see, the hardness of the samples remains unaffected for temperatures below 200°C at 120HV. After that, the hardness reduces to 80 HV for temperatures between 200 and 300°C where it remains for the higher temperatures. This response can be explained if we observe the TEM microscopy of the material for temperatures between 200 and 400°C. The TEM micrographs(Figure 78) show that the microstructure of the base metal consists of small precipitates. During the simulation at 200°C those precipitates remain unaffected. However, at the temperature of 300°C, dissolution occurs which causes the and growth of the precipitates. Further heat at 400°C causes full dissolution of the precipitates
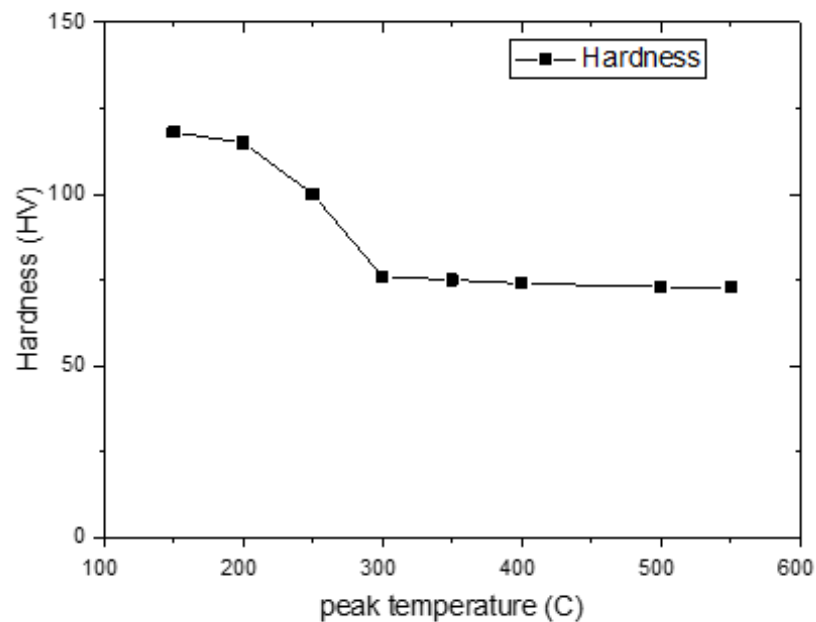

Figure 77: Hardness as a function of peak temperature of simulated specimens.
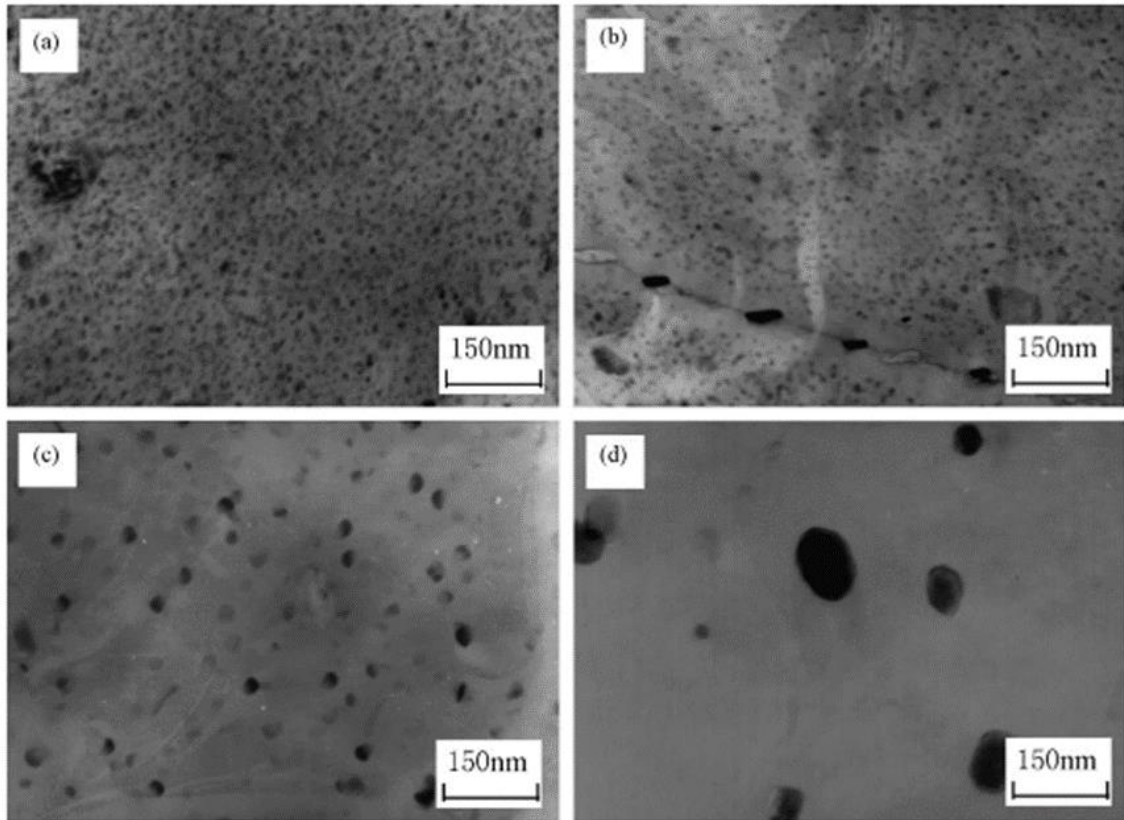
Figure 78 : TEM micrographs directly after heat treatments depending the peak temperature a) base metal b)200°C c)300°C d)400°C [29].

Following the above observation, we can assume that the softening of the heat affected zone can be due to the following two factors:

- Dissolution of precipitates
- Growth of precipitates

In order understand the effect of those two mechanisms, we artificially aged the samples at 120°C for 24 hours. The results of the new microhardness after the ageing are presented in the Figure 79. As we can observe the hardness responds in two ways. For temperatures between 300 and 400°C the microhardness hasn't significantly changed after the ageing process. Especially at 350°C it is totally unaffected. For the rest of the temperatures, the hardness has elevated to the initial values of the base metal. As a result of those observations we can assume that above 400°C the hardness fully recovers to the hardness of the base metal due to the age treatment, but for temperatures between 300 and 400°C overageing occurs making the ageing ineffective. Therefore, the heat affected zone can be divided in two parts, the dissolution zone and the overageing zone .
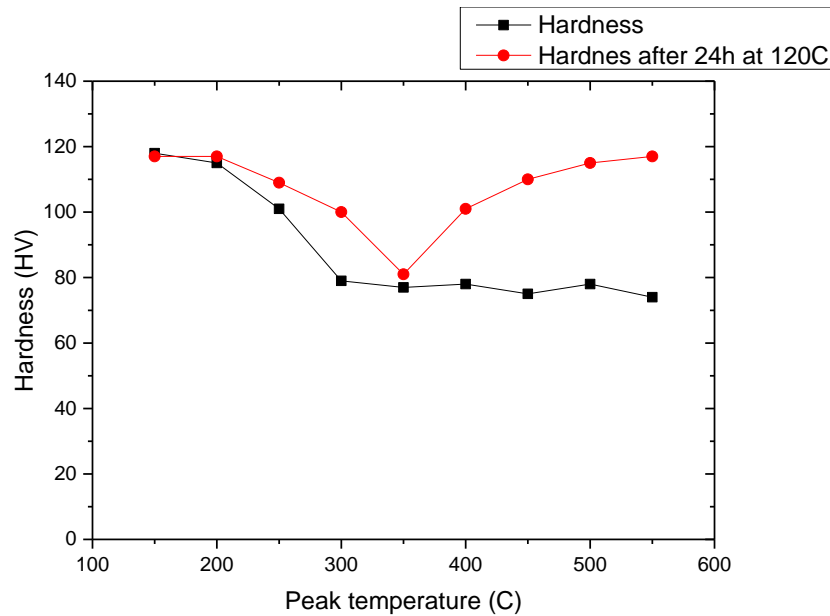
Figure 79 : Hardness profile of the HAZ simulated samples before and after artificial ageing.

4.4.3   Microhardness measurements of post weld heat treatments of the entire 7005-T6 weld.

In order to examine the effect of the post weld heat treatment on the entire 7005 weld, we used the ageing process that were described in section 3.3.1.

- Natural ageing for 1 year
- Artificial ageing for 12 hours at 120°C.
- Artificial ageing for 24 hours at 120°C.
- Artificial ageing for 42 hours at 120°C.

For the natural ageing for 1 year, the microhardness profile compared to non-aged weld profile, is as follows.
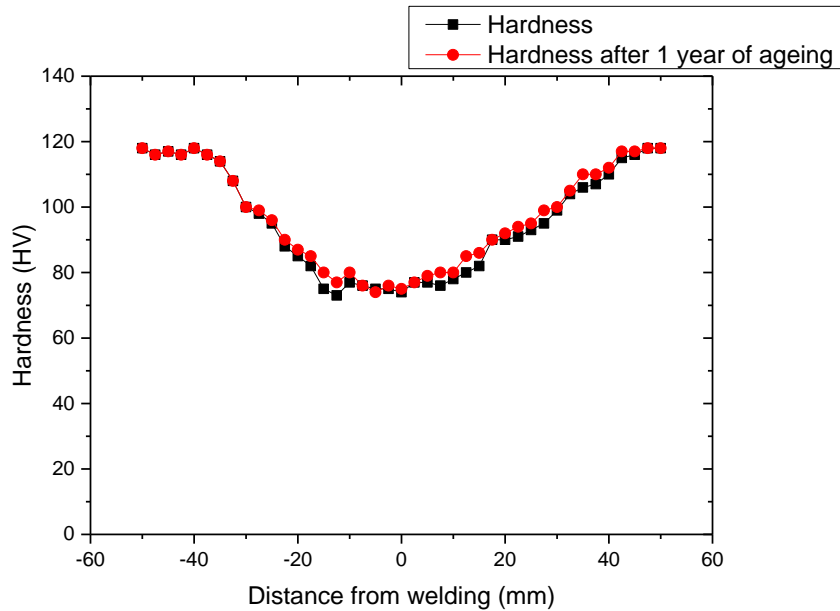
Figure 80 : Microhardness profile of natural aged process compared to non-aged.

As we can see in the figure above the natural ageing of the weld hasn't changed its hardness even one year after the welding has occurred.

The microhardness results for the artificial ageing are presented in the following figure.
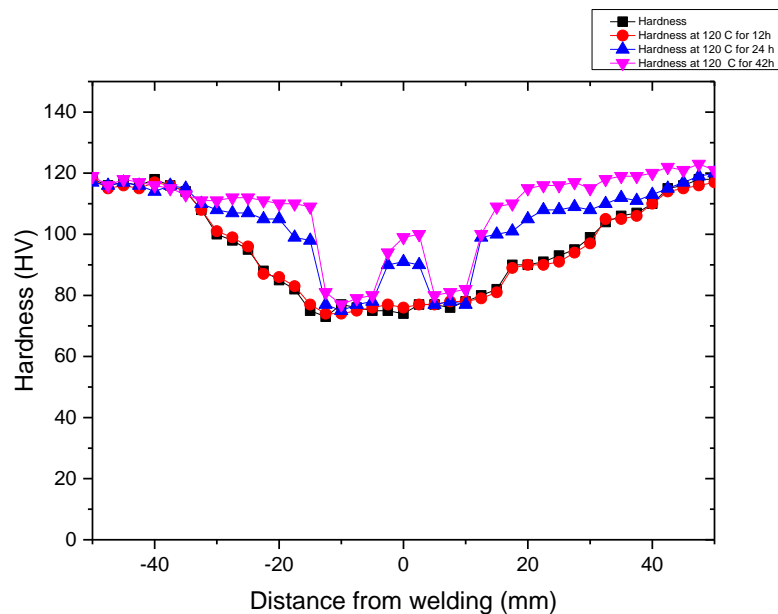
Figure 81 : Microhardness profile of the 7005-T6 after artificial ageing

As illustrated in the figure above, the microhardness of the weld has been affected by the artificial ageing. For the 12 hours at 120°C the hardness hasn't been affected by the ageing process, but after 24 hours we can observe a significant elevation of the hardness in the heat affected zone. Again, as in the previous section there is the part of the HAZ that isn't affected and represents the overageing zone (distance between 5 and 10 mm from the welding). At 42

hours this effect is even more clear as the hardness of the heat affected zone has reached the hardness of the base metal.

At Figure 82 we can see the profile of the microhardness of the step ageing, which consist of: 8 hours at 120°C followed by 24 hours as at 150°C. As we can observe, the hardness of the heat affected zone far from the welded metal remains low, indicating that the step ageing isn't affecting its microhardness.
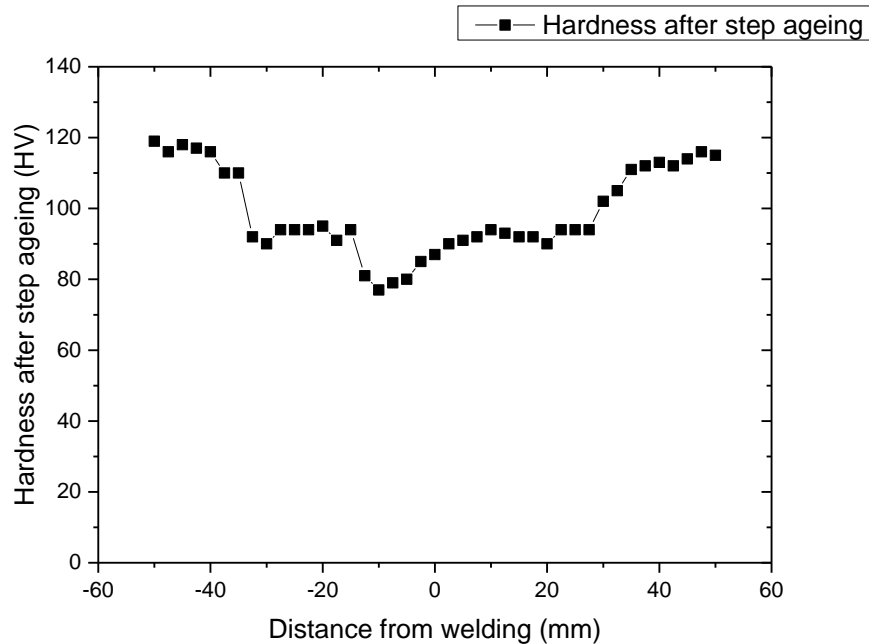
Figure 82 : Hardness profile of step ageing for 8 hours at 120°C followed by 24 hours as at 150°C.

4.5   Thermocalc - Scheil

Thermodynamic calculations of the proposed chemical composition mentioned in Table 2 were performed with Thermo-Calc and TCAL5 database as well as Scheil calculations for the evaluation sequence of the precipitates.

More specifically, Figure 83 presents the phase diagram of the Al-Mg-Zn by presenting the Al-Zn and Al-Mg phase diagrams.

(a)   (b)
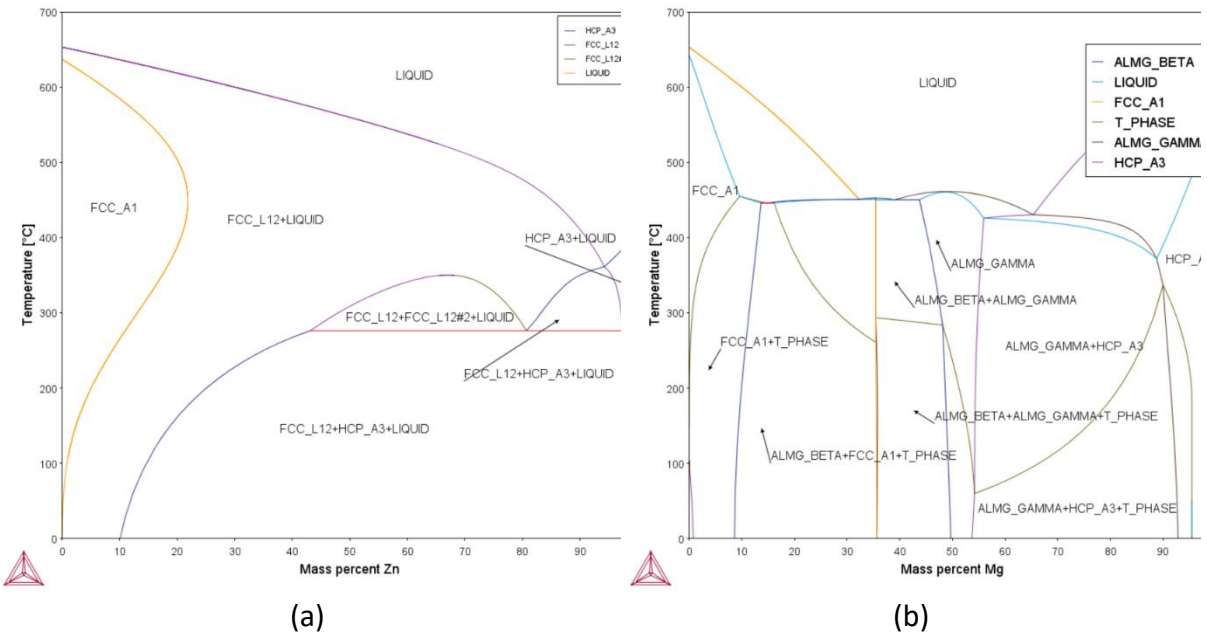
Figure 83: Phase diagram for Al-Mg-Zn system showing the different phases that appear in thermodynamic equilibrium. a) Al-Zn b) Al-Mg

For better specification of the precipitates and the compounds, the ternary diagram of the Al-Mg-Zn system is presented bellow for temperatures of 120,200,400 and 500 °C in Figure 84. Figure 85 and Figure 86 illustrate the Scheil calculation of alloy 7005 and Al alloyAl-Mg-Zn.

(a)   (b)

(c)   (d)
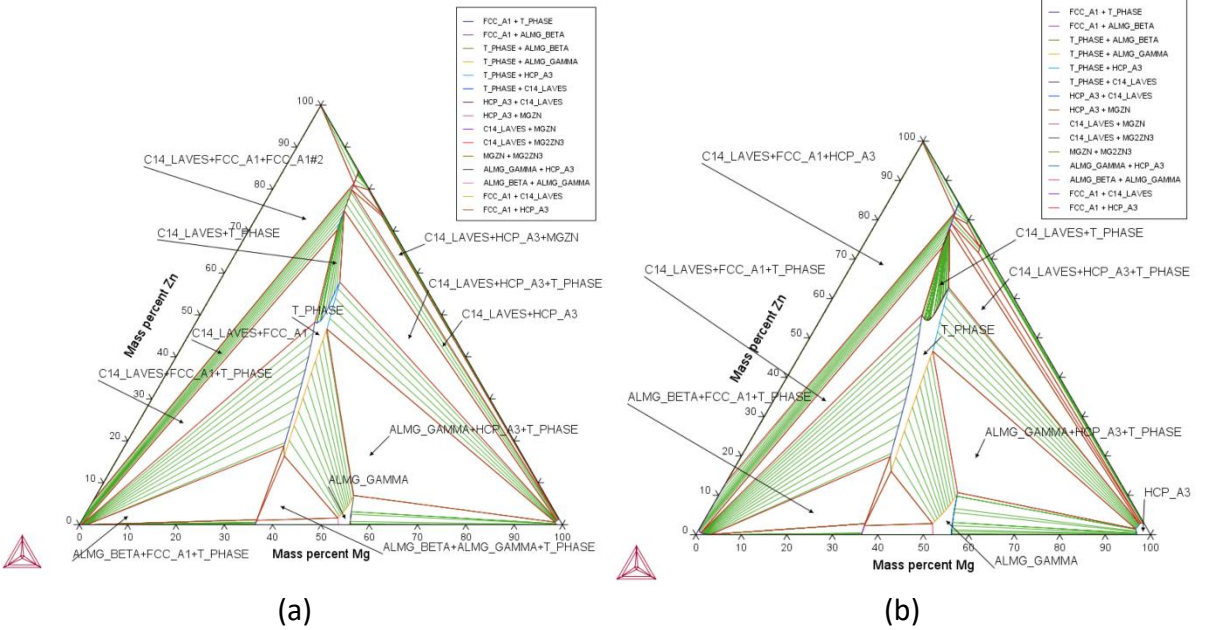
Figure 84: Al-Mg-Zn ternary diagram for a) 120°C, b) 200°C, c) 400°C d) 500 °C
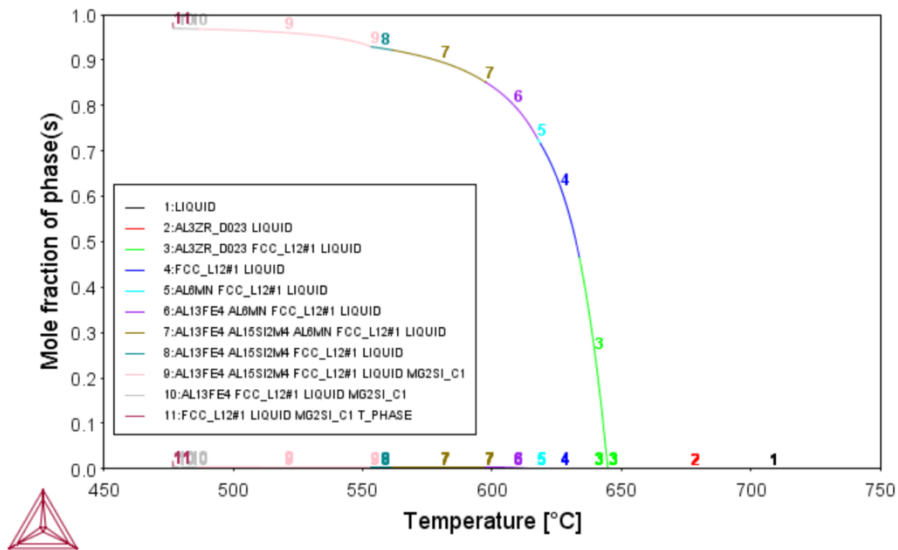
Figure 85: Scheil 7005 -Mole fraction of phases-Temperature(^{0}C)
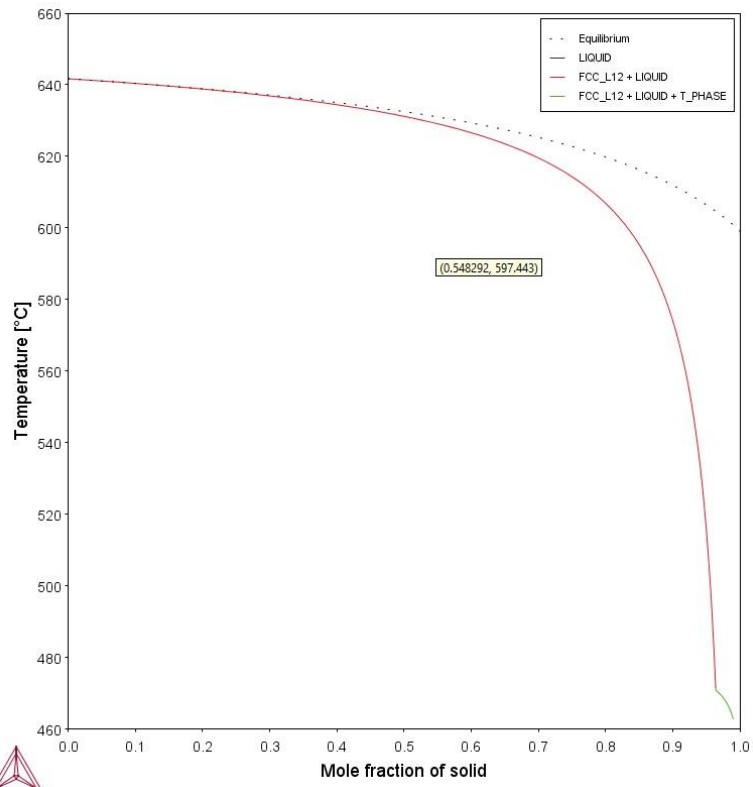
Figure 86: Scheil Al-Mg-Zn

5   Conclusions

During the present thesis several conclusions were reached.

- The hardness profiles of the 7005 and 7020 have a similar respond to the heat input.
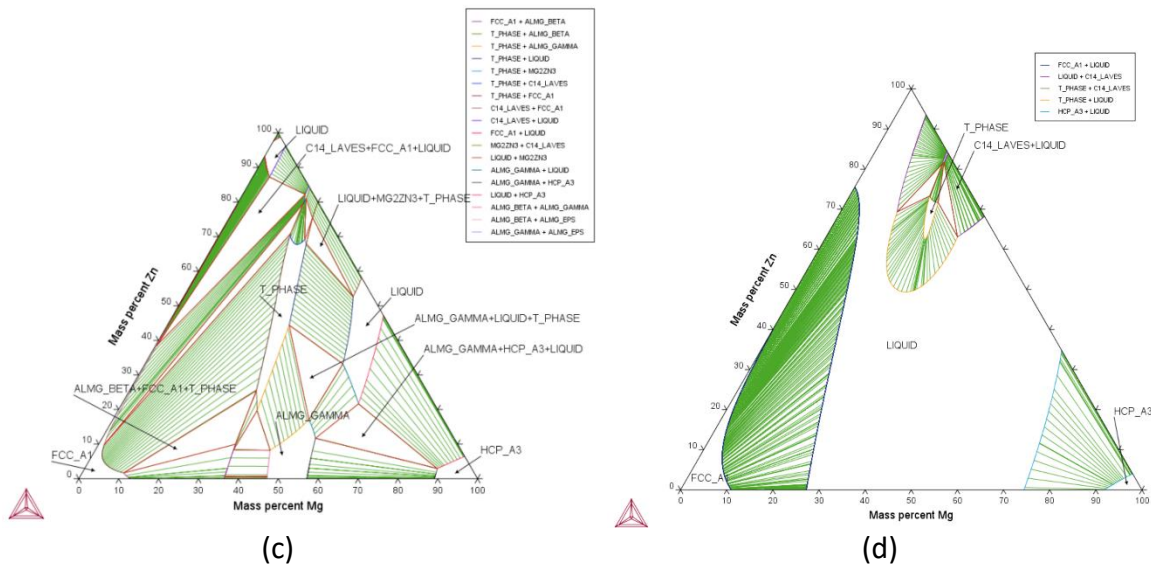- The heat affected zone of the 7005-aluminum alloy can by sub-divided in two zones depending the hardness mechanisms: The overageing zone and the dissolution zone
- The overageing zone consists of precipitates that are grown in temperatures between 300°C and 400°C.
- The dissolution zone consists of dissolution precipitates that form for temperatures over 400°C.
- The hardness of the heat affected zone can be recovered by post weld heat treatment. Among the post weld heat processes the most effective one is heating at 120°C for 42h.

6 References

1. Davis, J.R., et al., *Aluminum and aluminum alloys*. 2010, Materials Park, OH: ASM International.

2. Polmear, I.J., *Light Alloys*. Third ed. Metallurgy and Materials Science Series, ed. R. Honeycombe and P. Hancock. 1995, London: Arnold. 362.

3. Aluminium alloy, in Wikipedia. 2020.

4. Understanding the Aluminum Alloy Designation System.

5. Kutz, M., W. John, and Sons, *Handbook of materials selection*. 2005, New York: John Wiley & Sons.

6. 7005 aluminium alloy, in Wikipedia. 2019.

7. Fukuda, T., *Weldability of 7000 series aluminium alloy materials.* Welding International, 2012. **26**(4): p. 256-269.

8. Azarniya, A., A.K. Taheri, and K.K. Taheri, *Recent advances in ageing of 7xxx series aluminum alloys: A physical metallurgy perspective.* Journal of Alloys and Compounds, 2019. **781**: p. 945-983.

9. Gladman, T., *Precipitation hardening in metals.* Materials Science and Technology, 1999. **15**(1): p. 30-36.

10. Ferragut, R., et al., *Precipitation kinetics in Al–Zn–Mg commercial alloys.* Journal of Materials Processing Technology, 2003. **141**(1): p. 35-40.

11. Smallman, R.E., Chapter 11 - Phase transformations I – precipitation hardening transformation, in Modern Physical Metallurgy (Fourth Edition), R.E. Smallman, Editor. 1985, Butterworth-Heinemann. p. 380-416.

12. Shan, D. and L. Zhen, 10 - Aging behavior and microstructure evolution in the processing of aluminum alloys, in Microstructure Evolution in Metal Forming Processes, J. Lin, D. Balint, and M. Pietrzyk, Editors. 2012, Woodhead Publishing. p. 267-297.

13. Stiller, K., et al., Investigation of precipitation in an Al–Zn–Mg alloy after two-step ageing treatment at 100° and 150°C. Materials Science and Engineering: A, 1999. **270**(1): p. 55-63.

14. Starink, M.J. and S.C. Wang, *A model for the yield strength of overaged Al–Zn–Mg–Cu alloys.* Acta Materialia, 2003. **51**(17): p. 5131-5150.

15. Berg, L.K., et al., *GP-zones in Al–Zn–Mg alloys and their role in artificial aging.* Acta Materialia, 2001. **49**(17): p. 3443-3451.

16. Pantelis, D.I., V.I. Papazoglou, and G.N. Haidemenopoulos, *Science and technology of weldings*. 2017: Tziolas.

17. Deschamps, A. and Y. Bréchet, *Influence of quench and heating rates on the ageing response of an Al–Zn–Mg–(Zr) alloy.* Materials Science and Engineering: A, 1998. **251**(1): p. 200-207.

18. Liu, M., B. Klobes, and K. Maier, *On the age-hardening of an Al–Zn–Mg–Cu alloy: A vacancy perspective.* Scripta Materialia, 2011. **64**(1): p. 21-24.

19. Liu, Y., S. Liang, and D. Jiang, Influence of repetitious non-isothermal aging on microstructure and strength of Al-Zn-Mg-Cu alloy. Journal of Alloys and Compounds, 2016. **689**: p. 632-640.

20. Degischer, H., et al., Decomposition processes in an Al–5% Zn–1% Mg alloy. II.– Electromicroscopic investigation. Z. Metallk., 1980. **71**: p. 231-238.

21. Komura, Y. and K. Tokunaga, Structural studies of stacking variants in Mg-base Friauf– Laves phases. 1980. **36**(7): p. 1548-1554.

22. Fernandez, P., et al., *Hardness-Lattice Parameter Correlation for Aged Al-Zn-Mg Alloys.* Journal of Materials Science & Technology, 2010. **26**(12): p. 1083-1088.

23. Patil, P.C. and M.R.D. Shelke. Experimental Investigation And Optimization Of Welding Parameters On Tig Welding Of 7005 Aluminium Alloy. 2016.

24. Sha, G., et al., *Growth related metastable phase selection in a 6xxx series wrought Al alloy.* Materials Science and Engineering A, 2001. **304-306**: p. 612-616.

25. Gómez de Salazar, J.M. and M.I. Barrena, *Role of Al2O3 particulate reinforcements on precipitation in 7005 Al-matrix composites.* Scripta Materialia, 2001. **44**(10): p. 2489-2495.

26. Belov, N.A., D.G. Eskin, and A.A. Aksenov, *Chapter 6 - Alloys with a High Content of Zinc*, in *Multicomponent Phase Diagrams*, N.A. Belov, D.G. Eskin, and A.A. Aksenov, Editors. 2005, Elsevier: Oxford. p. 193-222.

27. Li, Y., X. Zhang, and X.-J. Ma. Microstructures and Mechanical Properties of MIG Welding Joint of 7005 Aluminum Alloy. 2016. Atlantis Press.

28. Ditta, A., et al., Microstructural characteristics and properties of spray formed Zn-rich Al-Zn-Mg-Cu alloy under various aging conditions. Materials Characterization, 2020. **161**: p. 110133.

29. Fu, G., F. Tian, and H. Wang, *Studies on softening of heat-affected zone of pulsed-current GMA welded Al–Zn–Mg alloy.* Journal of Materials Processing Technology, 2006. **180**(1): p. 216-220.